



HAL
open science

Measuring the viscosity of lava in the field: A review

Magdalena Oryaëlle Chevrel, Harry Pinkerton, Andrew J.L. J.L. Harris

► To cite this version:

Magdalena Oryaëlle Chevrel, Harry Pinkerton, Andrew J.L. J.L. Harris. Measuring the viscosity of lava in the field: A review. *Earth-Science Reviews*, 2019, 10.1016/j.earscirev.2019.04.024 . hal-02150640v2

HAL Id: hal-02150640

<https://hal.science/hal-02150640v2>

Submitted on 13 Apr 2020 (v2), last revised 7 Mar 2023 (v3)

HAL is a multi-disciplinary open access archive for the deposit and dissemination of scientific research documents, whether they are published or not. The documents may come from teaching and research institutions in France or abroad, or from public or private research centers.

L'archive ouverte pluridisciplinaire **HAL**, est destinée au dépôt et à la diffusion de documents scientifiques de niveau recherche, publiés ou non, émanant des établissements d'enseignement et de recherche français ou étrangers, des laboratoires publics ou privés.

Measuring the viscosity of lava in the field: A review

Magdalena Oryaëlle Chevrel^{a*}, Harry Pinkerton^b, Andrew J.L. Harris^a

^aUniversité Clermont Auvergne, CNRS, IRD, OPGC, Laboratoire Magmas et Volcans, f-63000 Clermont-Ferrand, France

^bLancaster Environment Centre, Lancaster University, Lancaster LA1 4YQ, United Kingdom

*Corresponding author: oryaelle.chevrel@gmail.com

Abstract

Many scientists who have worked on active lava flows or attempted to model lava flows have recognized the importance of rheology in understanding flow dynamics. Numerous attempts have been made to estimate viscosity using flow velocities in active lava channels. However, this only gives a bulk or mean value, applies to channelized flow, and the need to estimate flow depth leads to a large degree of uncertainty. It is for this reason that some scientists resorted to more direct methods for measuring the lava viscosity in the field. Initial attempts used crude instruments (such as forcing a rod into a flow using the operators body-weight), and even the latest instruments (motor-driven rotational viscometer) are significantly less refined than those one would encounter in a well-equipped laboratory. However, if suitable precautions are taken during instrument design, deployment in the field and post-processing of data, the results form an extremely valuable set of measurements that can be used to model and understand the complex rheological behavior of active lava flows. As far as we are aware, eleven field measurements of lava rheology have been published; the first took place in 1948, and the latest (at the time of writing) in 2016. Two types of instrument have been used: penetrometers and rotational viscometers. Penetrometers are suitable for relatively high viscosity (10^4 - 10^6 Pa s) lava flows, but care has to be taken to ensure that the sensor is at lava temperature and measurements are not affected by the resistance of outer cooled crust. Rotational viscometers are the most promising instruments at lower viscosities (1 - 10^4 Pa s) because they can operate over a wider range of strain rates permitting detailed flow curves to be calculated. Field conditions are challenging and measurements are not always possible as direct approach to and contact with active lava is necessary. However it is currently the only way to capture the rheology of lava in its natural state. Such data are fundamental if we are to adequately model and understand the complex behavior of active lava flows.

34

35 **Keywords**

36 Lava flow, Rheology, Field Viscometry, Shear Stress, Strain Rate, Viscosity, Yield Strength,
37 Penetrometer, Rotational viscometer

38 **1 Introduction**

39 Lava flow dynamics and flow length are influenced by a number of factors including effusion
40 rate at the vent, ground slope, channel dimensions, flow velocity, eruption duration, insulation
41 and, critically, the rheology of the lava (e.g., Walker 1973; Pinkerton and Wilson 1994;
42 Keszthelyi and Self 1998; Griffiths 2000; Harris et al. 2005; Kerr and Lyman 2007; Harris
43 and Rowland 2009; Castruccio et al. 2013). During an eruption, estimates of the effusion rate
44 and mean ground slope can be made, and these can be used as source terms in lava flow
45 emplacement models to assess potential hazards (e.g., Vicari et al., 2011; Ganci et al., 2012;
46 Mossoux et al., 2016; Coppola et al., 2017). However, the rheological properties of the
47 flowing and modeled lava are subject to major uncertainties. Current lava flow models (e.g.,
48 Crisci et al. 1986; Harris and Rowland 2001; Hidaka et al. 2005; A Vicari et al. 2007; Herault
49 et al. 2009; 2011; Bilotta et al. 2014; Kelfoun and Vargas 2016; Chevrel et al. 2018a) use
50 rheological data that are either unchanging during flow development or vary down flow as a
51 function of evolving temperature and crystal content. However, these do not accurately reflect
52 the behavior of lava during emplacement because they neglect the effects of volatile content,
53 oxygen fugacity, cooling rate, degassing, strain rate and bubble growth.

54 Lava is composed of crystals and bubbles in suspension in a silicate liquid and its
55 rheology depends on the viscosity of the liquid phase and on the effect of the particles
56 (bubbles and crystals) it contains (cf. Pinerton and Stevenson 1992; Crisp et al., 1994;
57 Cashman et al., 1999; Mader et al., 2013). The viscosity therefore changes down flow because
58 lava temperature, bubble content and crystallinity evolve as functions of both time (i.e., as
59 eruption progresses) and space (i.e., with distance from the source) (Lipman et al., 1985;
60 Lipman and Banks, 1987; Moore, 1987; Crisp et al., 1994; Cashman et al., 1999; Soule et al.,
61 2004; Riker et al., 2009; Chevrel et al., 2013; Robert et al., 2014; Rhéty et al., 2017). Upon
62 eruption, the liquid phase is Newtonian and its viscosity depends on chemical composition
63 (including major elements and volatiles) and temperature. The viscosity of silicate melts is
64 relatively easily measured as a function of temperature in the laboratory and composition-
65 based empirical models have been established (e.g., Bottinga and Weill, 1972; Shaw, 1972;

66 Hess and Dingwell, 1996; Giordano and Dingwell, 2003; Hui and Zhang, 2007; Giordano et
67 al., 2008; Sehlke and Whittington, 2016). In contrast, the effect of particles is more difficult
68 to quantify because the mixture becomes non-Newtonian and yield-strength, shear thinning
69 and thixotropic behavior may appear. The mixture (melt + particles) rheology depends on
70 particle concentration, aspect ratio (for crystals), ability to deform (for bubbles), size
71 distribution, shear stress and applied strain rate (Barnes, 1989; Larson, 1999). The effect of
72 particles has been estimated via several theoretical and empirical models based on
73 experiments of analogue material (e.g., Einstein, 1906; Krieger and Dougherty, 1959; Maron
74 and Pierce, 1956; Costa et al., 2009; Mueller et al., 2010; Castruccio et al., 2010; Cimarelli et
75 al., 2011; Moitra and Gonnermann, 2015; Klein et al., 2018). These have been applied to
76 constrain lava flow rheology in several studies (Pinkerton and Stevenson, 1992; Crisp et al.,
77 1994; Cashman et al. 1999; Guilbaud et al., 2007; Harris and Allen, 2008; Riker et al., 2009;
78 Chevrel et al., 2013; Le Losq et al., 2015; Castruccio and Contreras, 2016; Chevrel et al.
79 2016; Rhéty et al., 2017). The effect of crystals has also been explored through crystallization
80 experiments of molten lavas (e.g., Ryerson et al. 1988; Pinkerton and Norton, 1995; Sato,
81 2005; Ishibashi and Sato, 2007; Vona et al., 2011; Vetere et al., 2013; Sehlke et al., 2014;
82 Soldati et al., 2014; Chevrel et al., 2015; Kolzenburg et al., 2016, 2017) and by deformation
83 of natural crystal-rich samples near the glass transition temperature (e.g., Caricchi et al., 2008;
84 Champallier et al., 2008; Cordonnier et al., 2009; Avard and Whittington, 2012; Lavallée et
85 al., 2012, 2007; Vona et al., 2013). The effect of bubbles on crystal-free lava rheology has
86 been investigated using analogue material or theoretically (e.g., Stein and Spera, 1992; Manga
87 et al., 1998; Lejeune et al., 1999; Saar and Manga, 1999; Bagdassarov and Pinkerton, 2004;
88 Rust and Manga, 2002a; Llewelin and Manga, 2005) as well as using bubble-bearing high
89 viscosity silicate melts near the glass transition (Bagdassarov et al., 1994; Bagdassarov and
90 Dingwell, 1993, 1992; Vona et al., 2016). The combined effect of bubbles and crystals has
91 been studied via laboratory experiments on magmas (Bagdassarov et al., 1994; Pistone et al.,
92 2016, 2013, 2012; Vona et al., 2017, 2016) and the three-phase theory (Phan-Thien and
93 Pham, 1997; Harris and Allen, 2008). Although laboratory measurements are well controlled,
94 they are not representative of field conditions because of differences in volatile content
95 (dissolved and in the form of gas bubbles), oxygen fugacity and crystallinity changes during
96 heating episodes in the laboratory. To generate realistic models of lava flow advance and to
97 place laboratory measurements in reference to nature, we thus need a basic knowledge of the
98 rheology of the molten mixture itself in its natural setting (i.e., in the field).

99 One method that is commonly used to obtain information on the rheological properties
100 of lavas in the field involves measuring the post-emplacement dimensions of the flows (e.g.,
101 Hulme, 1974; Moore and Schaber, 1975; Fink and Zimbelman, 1986; Moore, 1987; Kilburn
102 and Lopes, 1991; Wadge and Lopes, 1991). Most of these studies are based on the assumption
103 that lavas can be approximated as Bingham fluids, and that their flow dimensions are
104 controlled by the yield strength and plastic viscosity. However, post emplacement subsidence,
105 complex lava flow fields and lava flow inflation may induce under- or over-estimation of
106 flow viscosity using this method (e.g. Kolzenburg et al., 2018c). Another method involves
107 measuring the mean velocity of lava in active channels to derive the rheological parameters. It
108 is often assumed that the lava behaves as a Newtonian fluid and the flow has a parabolic
109 velocity profile. In that case, the Jeffreys (1925) equation is applied to calculate the viscosity
110 (e.g., Nichols, 1939; Krauskopf, 1948; Walker, 1973; Rose, 1973; Harris et al., 2004; James
111 et al., 2007). Other studies showed that non-Newtonian flow behavior is preferable and
112 consider a plug-flow model to extract yield strength and viscosity (e.g., Cigolini et al., 1984;
113 Moore, 1987; Harris et al., 2002; Balmforth et al., 2007;). An additional field method can be
114 used when flows undergo super-elevation when they encounter sharp bends in channels
115 (Heslop et al., 1989; Woodcock and Harris, 2006). Unfortunately, there are few situations
116 where this method can be applied. All these methods are based on the whole flow behavior,
117 and therefore, suffer from potentially large uncertainties due to difficulties to measure channel
118 shape, depth, lava density and underlying slope (cf. Hon et al., 2003; Lefler, 2011; Chevrel et
119 al., 2013; Lev and James, 2014; Kolzenburg et al., 2018b). In addition, the calculated
120 properties are not necessarily representative of the viscosity of the material itself but represent
121 the behavior of the flow as a whole (fluid interior plus brittle and viscoelastic crust).
122 Consequently, to constrain the rheological parameters of lava in its natural state, we must use
123 field-based instrumentation.

124 The only way to directly establish lava rheology in the field is to measure it by
125 inserting a viscometer into the flowing molten rock. If this technique is applied down an
126 active channel and is combined with simultaneous temperature measurement and sampling, it
127 is possible to capture the evolution of lava rheology as a function of cooling, degassing and
128 crystallization. However, *in-situ* viscosity measurements are challenging due to the difficulty
129 of approaching an active lava flow, and the problems of designing equipment that will make
130 reliable measurements under such difficult conditions. Besides, during eruption, lava flows
131 are continuously changing (advancing, cooling, degassing, advecting) therefore the

132 measurement timescales needs to be adapted with the timescale for which the lava is at
133 constant conditions (mainly temperature). This is often a limitation for the measurements
134 because low torques and low deformation rates are difficult to reach due to the fast thermal
135 dynamics. As a result, only a small number of investigators have accepted the challenge of
136 measuring the rheological properties in the field. Their studies are reported here. In this
137 article, we thus review how rheological properties can be measured using field
138 instrumentation. We then collate all field viscometry experiments made to date in
139 chronological order. For each of these eleven cases found, we include a discussion of the field
140 conditions, and instrument description, and review the main results and conclusions.

141 **2 Measuring lava rheology in the field**

142 **2.1 Methods and theory**

143 Quantification of rheology is described by the relationship between the applied stress, and the
144 rate of deformation i.e. strain rate. These quantities are measured using a viscometer. There
145 are essentially two types of viscometer that have been used to measure the rheological
146 properties of lava in the field. One measures the resistance to penetration of an object, which
147 moves into the lava, and the other measures the torque required to rotate a shear vane that is
148 immersed in the lava. These viscometers are based on the principle of applying either a stress
149 or a strain rate while measuring the response either of the strain rate or the stress. When using
150 a rotational viscometer, the shear strain rate is a function of the rotation rate and the geometry
151 of the vane. For a penetrometer it is a function of the penetrometer head shape and the axial
152 penetration rate. Shear stress is a function of the torque acting on the rotating spindle or the
153 force acting on the penetrating head. If the rotational viscometer or penetrometer has the
154 ability to vary the speed of rotation or penetration, or the applied force, a graph of strain rate
155 versus stress can be constructed to produce, following the term given by Lenk (1967), “flow
156 curves”. Depending on the lava properties being measured, one of the following rheological
157 models can be fitted to the data (see Chapter 5 in Chester et al., 1986). All parameters used
158 for the following equations are given in Table 1.

159 For Newtonian behavior, the strain rate ($\dot{\gamma}$) is directly proportional to shear stress (τ). The
160 proportionality coefficient is the viscosity (η) and is defined by:

$$\tau = \eta \dot{\gamma} \quad (1)$$

161 Bingham behavior is identified when a minimum stress (i.e., the yield strength, τ_0) needs to
162 be overcome before deformation occurs. In that case, once the yield strength is overcome, the
163 strain rate is proportional to shear stress. The proportional coefficient is the consistency (K),
164 otherwise termed the Bingham or plastic viscosity. This is defined via:

$$\tau = \tau_0 + K\dot{\gamma} \quad (2)$$

165 When strain rate is not proportional to shear stress, and the lava has no discernible yield
166 strength, the material is best characterized as a power law flow, defined as:

$$\tau = K\dot{\gamma}^n \quad (3)$$

167 where, if n , the flow index, equals unity this reduces to the Newtonian case (Eq. 1).

168 The last rheological model used to describe lava behavior, is when a minimum stress is
169 present and once it is overcome the shear stress follows a power law with strain rate. This is
170 termed the Herschel-Bulkley model and described by:

$$\tau = \tau_0 + K\dot{\gamma}^n \quad (4)$$

171 For all fluids, the value of n in Eqs. 3 and 4, is evaluated graphically or numerically from the
172 experimentally determined values of strain rate and shear stress. When $n > 1$, the fluid is
173 dilatant (also termed shear thickening), i.e. viscosity increases with strain rate. Evidence for
174 this behavior has been found in dykes (Smith, 1997, 2000), but has yet to be encountered in
175 flowing lava. When $0 < n < 1$, the material is thinning with deformation, so that viscosity
176 decreases with strain rate. In that case, the fluid follows a pseudo-plastic behavior. After a
177 few percent of crystallization, it has been recognized that lavas preferentially follow this
178 behavior (Pinkerton and Stevenson, 1992).

179 **2.2 Instrumentation**

180 **2.2.1 Penetrometers**

181 There are three types of penetrometer. A “simple” penetrometer is based on a penetrometer
182 used for measurement of soil physical properties (Lunne et al., 1997) and is basically a metal
183 rod, with a semi-spherical head, pushed into the lava. Penetrometers can be used to measure
184 yield strength by establishing the minimum force required to initiate movement (Pinkerton
185 and Sparks, 1978) or can be used to estimate viscosity by inserting the rod into the lava at a
186 given constant force and recording the speed of penetration (Einarsson, 1949, 1966; Gauthier,
187 1973; Pinkerton and Sparks, 1978; Panov et al. 1988; Belousov and Belousova, 2018). Using

188 a semi spherical penetration head and assuming that the potential effect of lava sticking to the
189 rod is negligible, the viscous drag is equal to half of Stokes' force acting on a sphere
190 penetrating through a viscous medium (Panov et al., 1988; Belousov and Belousova, 2018).
191 The lava viscosity is then calculated via:

$$\eta = \frac{F}{3\pi u R_{eff}} \quad (5)$$

192 where F is the force of penetration (viscous drag), u is the speed of penetration, and R_{eff} is the
193 effective radius of the rod. The force is recorded by a hand gauge and the velocity is measured
194 from the penetration depth and time to reach that depth. This results in a single viscosity
195 measurement point, which is averaged over the duration of penetration. For a given
196 penetration depth the viscosity may then be obtained from prior calibration (Einarsson, 1966,
197 1949; Gauthier, 1973; Pinkerton and Sparks, 1978).

198 The second type of penetrometer is termed "ballistic" penetrometer as used by
199 Gauthier (1971, 1973). This technique involves shooting a spear at high-speed
200 perpendicularly into the lava and measuring its penetration depth. The viscosity is then
201 calculated based on previous laboratory calibrations using the same spear on various liquids
202 of different viscosities. The high initial penetration velocity prevents lava advance rates from
203 influencing the measurement and limits cooling of the lava around the spear during
204 penetration. The major disadvantage of such penetrometers is that they are inserted through
205 the outer, cooled part of a flow, thus the force required to penetrate the lava is the result of a
206 summation of shear stresses induced within the thickness penetrated, the major resistance to
207 shearing being due to the more viscous outer (crusted) regions. This penetrometer thus tends
208 to give a semi-quantitative measurement of the shear strength of the cooler exterior of a flow,
209 and little indication of the rheological characteristics of the hot interior.

210 This problem can be overcome using a third type of penetrometer that is first
211 preheated and inserted through the cooled outer regions before being activated, so only the
212 nose of the penetrometer that had been placed into the flow interior is moved forward
213 (Pinkerton and Sparks, 1978). This instrument used a compressed spring as the energy source
214 for penetration. The controlled reduction in axial force during penetration was recorded,
215 together with the simultaneous piston advance rates. This type of dynamic penetrometer
216 permitted the shear stress - strain rate characteristics of the lava to be determined using the
217 method outlined in Pinkerton (1978).

218

Symbol	Description	Unit
η	Viscosity	Pa s
τ	Shear stress	Pa
$\dot{\gamma}$	Strain rate	s ⁻¹
τ_0	Yield strength	Pa
K	Consistency	Pa s
n	Flow index	
<i>Penetrometer</i>		
F	Force of penetration	N
u	Speed of penetration	m s ⁻¹
R_{eff}	Effective radius of the rod	m
<i>Rotational viscometer</i>		
M	Torque	N m
Ω	Angular velocity	rad s ⁻¹
h	Vane length	m
Ri	Vane radius	m
Ro	Container radius	m

220 **Table 1:** Notation of parameters and units

221

222 2.2.2 Rotational viscometer

223 Rotational viscometers involve a rotating spindle immersed into the molten lava. Two types
 224 of rotational viscometer have been employed in the field: a fixed rig sited on the top of a lava
 225 lake (Shaw et al., 1968) and a portable instrument inserted by hand through the flow surface
 226 and into the lava interior (Pinkerton, 1994; Pinkerton et al., 1995a, 1995b; Pinkerton and
 227 Norton, 1995; Chevrel et al., 2018a). In use, the spindle can be operated in either controlled
 228 strain rate or controlled shear stress mode. The theory employed with this instrument is that of
 229 wide-gap concentric cylinder viscometry where the torque is converted into shear stress and
 230 the rotational speed into strain-rate using the spindle geometry via the Couette theory, which
 231 is similar to the theory used for the laboratory viscometers described in Dingwell (1986) and
 232 Spera et al. (1988). Unlike most laboratory experiments where the immersed spindle is
 233 cylindrical, vane geometry is commonly used in the field to lower the weight, ease
 234 penetration, reduce disturbance of lava during insertion, minimize the effects of cooling and
 235 reduce slippage between the edge of the vane and the lava. The material between the vanes is
 236 trapped and therefore a virtual cylinder of sample material is used for the calculation. The
 237 shear stress is then calculated via:

$$\tau = \frac{M}{2\pi h R_i^2} \quad (6)$$

238 where M is torque, h is vane length and R_i is the radius of the rotating cylinder (or equivalent
239 radius of the vane). The strain rate is obtained from the angular velocity of the rotating vane
240 via (Stein and Spera, 1998):

$$\dot{\gamma} = \frac{2\Omega}{n \left(1 - \left(\frac{R_i}{R_o}\right)^{2/n}\right)} \quad (7)$$

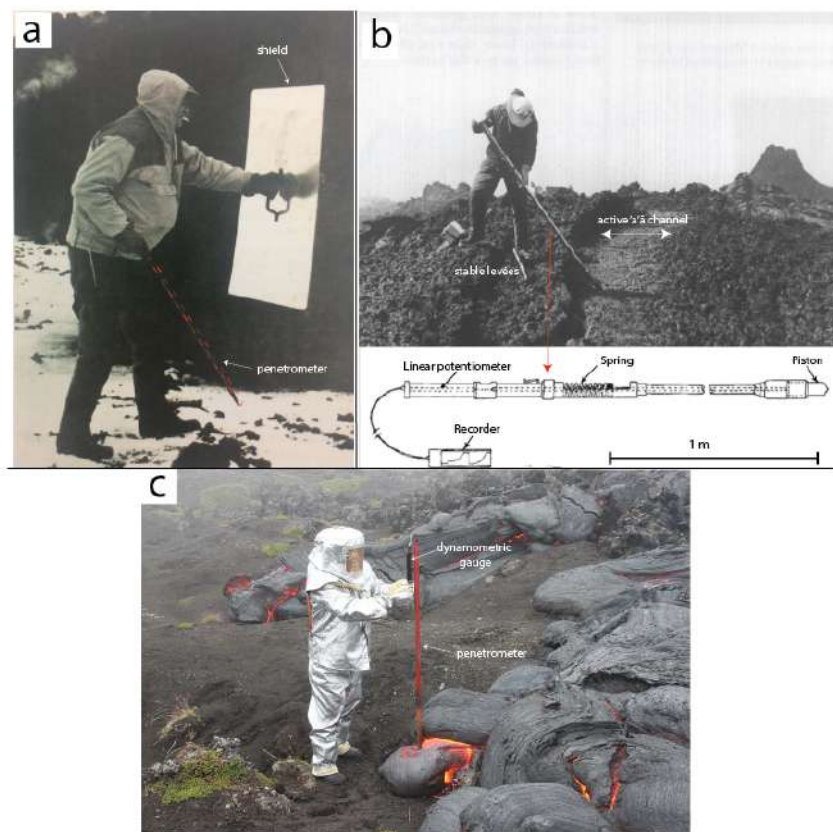
241 where Ω is angular velocity, n is flow index (obtained by calculating the slope of the
242 measured $\ln(\tau)$ against $\ln(\Omega)$), and R_o is the radius of the outer cylinder.

243 **3 Review of lava viscometry experiments in the field**

244 **3.1 An iron rod thrust into the lava by Einarsson (1949) at Hekla, Iceland**

245 While observing lava emplacement on Hekla in 1948, Einarsson quickly realized that the lava
246 presented interesting changes in vesicularity, temperature, crystallinity and apparent viscosity
247 (Einarsson 1949). To measure viscosity, he used a simple iron rod and thrust it by hand into
248 the lava. Einarsson applied a force on the rod manually and measured the time needed to
249 penetrate the lava. From a qualitative approach, he could “feel” different behaviors. The most
250 fluid lava allowed him to push the iron rod in with one hand, which reached depth of 20 to 30
251 cm in one or two seconds. In the most viscous lava, he could thrust the rod only 2-3 cm into
252 the flow (also in 1 to 2 s) and this was achieved by putting his whole body weight onto the
253 rod. To quantify viscosity, back into the laboratory, Einarsson established a relationship
254 between viscosity and velocity of penetration from repeated measurements using the iron rod
255 plunged into a hot mixture of Trinidad asphalt and asphalt oil. He estimated the viscosity of
256 the lava at Hekla to be between 5×10^4 Pa s and 1.5×10^6 Pa s, and he estimated an error of
257 about half order of magnitude. The erupted lavas were basaltic-andesite (55 wt.% SiO₂) and
258 were described as ‘a’ā to block type. The maximum temperature was estimated using an
259 optical pyrometer as 1150°C (Einarsson 1949). Analyses of the lava texture revealed that the
260 low viscosity values corresponded to “spongy, uncrystallized fluid”, while the high viscosity
261 value corresponded to denser lava. Einarsson (1949) concluded that accurate measurements of
262 viscosity using this technique on this type of lava are difficult because of the lack of time
263 available to make instrumental measurements and because of hazards arising from blocks

264 falling from the steep rubbly flow margin and high radiant heat. In 1961, Einarsson intended
265 to measure the lava viscosity at Askja (Iceland; Fig. 1a) but no data were recorded.



266
267 **Figure 1:** a) Einarsson holding the penetrometer in one hand and a shield in another hand, advancing toward
268 the lava flow during Askja (Iceland) eruption in 1961 (photo modified from Solbnes et al. 2013). b) Pinkerton
269 using the penetrometer Mark 2 on a small channelized ‘a’ā flow of Mont Etna (Italy) in 1978 (sketch modified
270 from Pinkerton and Sparks, 1978). c) Belousov using a lava-penetrometer equipped with a dynamometric gauge
271 on a pāhoehoe lobe during the Tolbachik (Russia) eruption in 2013 (modified from Belousov and Belousova
272 2018).

273 3.2 Viscosity measurement at Surtsey, Iceland, by Einarsson (1966)

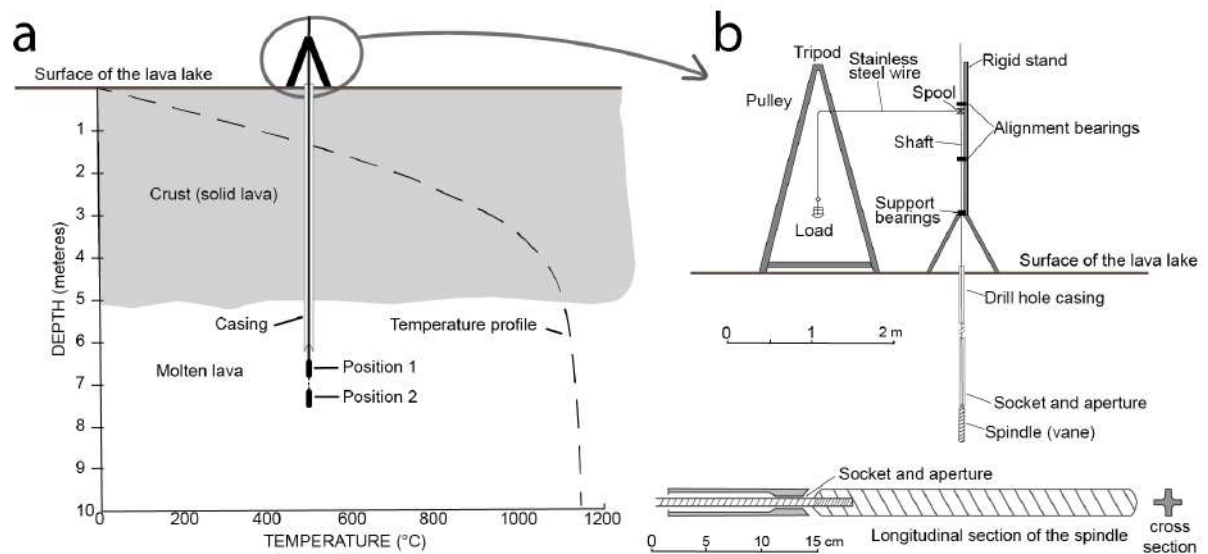
274 During the Surtsey eruption in 1964, Einarsson measured the viscosity of the flowing lava
275 using the same approach as he applied at Hekla in 1948 (Einarsson 1966). Einarsson
276 mentioned that this time the measurements were difficult to perform because the lava was too
277 fluid. Because the penetrometer was pushed by hand, it was difficult to regulate the force of
278 penetration to a minimum in order to measure the resistance of the fluid lava. After several
279 attempts, Einarsson estimated that the penetrometer moved 10 cm vertically into the lava at
280 the front of a lava lobe under its own weight in 0.5 s from which he obtained a viscosity
281 estimation of 5×10^2 Pa s. Einarsson noticed that this value was lower than expected because
282 he estimated viscosity at 10^3 Pa s from lava wave amplitudes in the lava lake located over the

283 vent. This underestimation was attributed to the “foamlike” texture of the lava. At that time,
284 Einarsson therefore sensed the potential effect of bubbles on lowering lava viscosity. The
285 samples of spatter that he collected showed about 45 vol. % of vesicles and 40 vol. % of
286 crystals (feldspar and olivine). The maximum temperature measured in the field with an
287 optical pyrometer was 1140 °C. Given these thermal and textural characteristics, a viscosity
288 value of 5×10^2 Pa s seems, therefore, appropriate.

289 **3.3 Viscosity measurements performed by Shaw et al. (1968) at Makaopuhi lava lake,** 290 **Hawaii**

291 Shaw et al. (1968) used the rotational viscometry method to determine the rheological
292 properties of lava at Makaopuhi lava lake in March 1965. Makaopuhi lava lake formed in 10
293 days by eruption of lava into a pit crater forming an 85 m deep and 800 m wide “pond”, and
294 after which the surface became stable and the upper part began to solidify. When the crust
295 reached a thickness of 2 m, cores were drilled periodically for temperature measurements and
296 lava sampling, as described in Wright and Okamura (1977). The viscosity measurements were
297 performed using one of the drill holes once the crust reached a thickness of about 4 m. The
298 experimental setup consisted of a support stand fixed on the top of the solidified lava lake
299 surface. A shaft, with a vane attached to its lower end, was suspended from the stand and
300 lowered vertically into the lava (Fig. 2). A casing was employed allowing the shaft to reach
301 the molten lava at the bottom of the cooled crust, where the temperature reached its maximum
302 (Fig. 2). A wire was spooled to the shaft, passed through a pulley and attached to a load,
303 permitting the shaft to rotate. In this way, by changing the load weight, different torques were
304 applied to the rotating vane. Flow curves were obtained by measuring the resulting rotational
305 speed (using stopwatches). The setup had been previously calibrated using petroleum asphalt
306 and uncertainties of 20 % on the viscosity were obtained. In the field, four different loads
307 were applied at two different depths (position 1 at 6.8 m and position 2 at 7.5 m) using the
308 same vane (Fig. 2). The temperature was measured at $1130 \pm 5^\circ\text{C}$ and sample analyses
309 revealed $< 5\%$ vesicles and 25 % of crystals. Viscometry results indicated that the lava was
310 non-Newtonian and thixotropic, which means that they observed a hysteresis between values
311 acquired during increasing and decreasing load (“up” and “down” curves, i.e. the “down”
312 stress-strain-rate path does not match the “up” path). Considering the up-curves, Shaw et al.
313 (1968) established that the Bingham model was the most appropriate to fit their data. They
314 estimated the yield strength to be 120 and 70 Pa, and obtained a plastic viscosity of 6.5×10^2
315 and 7.5×10^2 Pa s, for positions 1 and 2, respectively over strain rates $0.1 - 1 \text{ s}^{-1}$. These

316 compare with values of 80 to 115 Pa s obtained for the lake interior by Wright and Okamura
317 (1977) by applying Stokes' Law to olivine crystal setting; the difference is likely due to the
318 latter estimate being for melt only and the former for a melt-crystal mixture. A re-analysis of
319 the Shaw et al. (1968) data suggested that no yield strength was present and that power law
320 models in the form of $\tau = 974 \dot{\gamma}^{0.75}$ and $\tau = 716 \dot{\gamma}^{0.54}$ provided a better fit with positions 1
321 and 2, respectively (Heslop et al., 1989).
322



323
324 **Figure 2:** Set-up of the viscosity measurements performed by Shaw et al. in 1968 at Makaopuhi lava lake,
325 Hawaii. Modified from Shaw et al. 1968. a) Schematic view of the stand fixed onto the top of the solidified lava
326 surface (thickness of the crust was of about 4-5 m at that time) showing the two positions where measurements
327 were performed and the temperature profile; b) zoom of the rotating viscometer device and spindle.

328
329 Shaw et al. (1968) also performed a falling sphere experiment. This experiment
330 consisted of a steel sphere attached to a fine stainless steel wire that passed through the same
331 casing used for the rotational viscometer. The sphere was released into the lava at its hottest
332 part and the movement of the wire behind the descending sphere provided information to
333 calculate the viscosity. However, they obtained only one measurement because in all other
334 attempts the wire broke before a measurement was taken. The apparent viscosity they
335 obtained via Stokes Law was 6×10^4 Pa s for a strain rate of 0.004 s^{-1} . Although this is larger
336 than values calculated using the power law models, it is consistent with pseudo-plastic
337 behavior.

338 These pioneering viscosity measurements are of uncontestedly good quality. However
339 the technique employed is appropriate only for stable lava lake with a thick crust.
340 Employment beyond such a setting is therefore limited.

341 **3.4 A shooting spear to measure lava viscosity on Mount Etna, Italy, by Gauthier**
342 **(1973)**

343 During the eruption of Mount Etna between 1969 and 1971, Gauthier (1971, 1973) performed
344 viscosity measurements using a crossbow to fire a ballistic penetrometer (a stainless steel
345 spear), into the lava flow. The penetrometer had an initial speed of 22 m/s. Based on
346 calibration, viscosity is determined from the final depth of penetration. The relation between
347 viscosity and penetration depth was established from laboratory experiments on materials
348 with different viscosities. The penetration depth was directly read from graduations on the
349 spear. In May 1971, Gauthier performed three sets of measurements. The first set was
350 completed during the first phase of the eruption at the lava flow front, 500 m from the vent.
351 Here, the viscosity was measured to be $\sim 1 \times 10^3$ Pa s and the temperature was 1050 °C.
352 Measurements on several incandescent blocks yielded $\sim 2.2 - 5.7 \times 10^3$ Pa s at a temperature
353 of 1080 °C. For other blocks, where the surface viscosity was clearly higher, estimates of
354 more than 10^7 Pa s were obtained for the outer few centimeters, $\sim 4.3 \times 10^3$ Pa s at 13 cm and
355 $\sim 8.5 \times 10^2$ Pa s at 33 cm. The second set of measurements, completed at the end of the first
356 eruptive phase at the vent resulted in a viscosity of $\sim 1.1 - 6.3 \times 10^5$ Pa s at a temperature of
357 1090 ± 14 °C. The third set of measurement was made at the beginning of the second eruptive
358 phase near the vent. Here, a temperature of 1128 °C and viscosity of $\sim 1.7 - 2.4 \times 10^3$ Pa s
359 was measured. A sample collected near the vent from a depth of 50 cm was analyzed. The
360 lava was a trachy-basalt with 44.6 vol.% of crystals, 22.8 vol.% of glass and 32.6 vol.% of
361 bubbles.

362 Although viscosity values were obtained from these measurements, Gauthier (1973)
363 concluded that “the objections to this method do not arise from difficulties of its application
364 in the field conditions, but from rheological interpretation of the length of penetration”.
365 Indeed, although the calibration fluids used in the laboratory had a vertical viscosity gradient
366 between the upper layer and the material core, they did not represent the same gradient as
367 natural lava. In other words, it was extremely difficult to calibrate the method by using a
368 similar viscous gradient to that found in a lava flow.

369 Gauthier (1971) also designed a simple penetrometer, which included a dynamometric
370 gauge and a thermocouple at the rod end. This instrument, when associated with video
371 footage, would allow measurement of the temperature of the lava and its viscosity as deduced
372 from the rate and depth of penetration. He believed that this rather simple and light-weight
373 method was well adapted for fieldwork. Unfortunately, it was never built.

374 **3.5 Field measurements of rheology of lava by Pinkerton and Sparks (1978) at Mount**
375 **Etna, Italy**

376 Pinkerton and Sparks (1978) deployed three instruments to characterize the rheological
377 properties of the lava flows erupted at Mount Etna during the 1975 eruption. The most
378 sophisticated was the “Mark 2” field viscometer. The Mark 1 was considerably heavier than
379 the Mark 2 and was used only once during the 1973 eruption on Heimay—with limited
380 success. It had two large (~100 mm diameter) pistons moving out of an even larger cylinder
381 that was inserted into the flow. It was extremely cumbersome and difficult to use, and
382 preheating it was a major issue. However, parts of the Mark 1 instrument were used in the
383 construction of the Mark 2.

384 The Mark 2 instrument was designed to overcome the problems with previous
385 penetrometer methods. The penetrometer’s head was protected from the cooler crust through
386 which it passed by an outer stainless steel tube. Once it had passed through the thermal
387 boundary layer and reached thermal equilibrium with the surrounding lava, it was propelled
388 into the flow by a compressed spring. This resulted in a gradually decreasing axial force being
389 applied and hence a decreasing shear stress being applied to the isothermal region adjacent to
390 the advancing piston (Fig. 1b). The position of the piston and hence velocity was recorded
391 using a hot wire pen recorder. On each occasion that the viscometer was used, the piston did
392 not extend fully, indicating that the lava had a measurable yield strength. Prior to field
393 deployment, the instrument had been calibrated in a viscous sucrose solution. The method
394 used to calculate the rheological properties is detailed in Pinkerton (1978). This first
395 instrument was employed 3 m down flow from the active vent. Measurements were made at a
396 depth of 20 cm where the temperature was 1086 ± 3 °C and the crystallinity of the flow
397 interior was 45 vol.%. More than 20 data points were obtained for shear rates < 0.15 s⁻¹. The
398 results indicated that the lava behaved in a pseudo-plastic manner, though it could be
399 approximated to a Bingham fluid at the applied shear rates. The best fit revealed a yield
400 strength of 370 ± 30 Pa and a plastic viscosity of $9.4 \times 10^3 \pm 1.5 \times 10^3$ Pa s.

401 The second instrument employed was a conventional penetrometer, which comprised a
402 2 m long, 3 cm diameter stainless steel rod. A pressure transducer allowed the axial force
403 during insertion to be measured. This instrument was used in a dynamic mode by measuring
404 the time taken by the pre-heated penetrometer to move 10 cm when inserted into the flow
405 interior under a range of applied axial forces. Methods used to calibrate this instrument and to
406 calculate rheological properties were similar to those used for the Mark 2 viscometer

407 (Pinkerton, 1978). One apparent yield strength measurement of 860 Pa was made at the same
408 point as the Mark 2 viscometer. This value is higher than the previous measurement due to
409 shear along the length of the shaft in contact with the outer thermal boundary layer and
410 confirms the limitations of simple penetrometers. Another yield strength measurement made
411 at a depth of 10 cm inside an advancing flow front was 6500 Pa at a temperature of 1045 °C.

412 The final instrument used was a stainless steel shear vane attached to a torque wrench
413 that allowed yield strength to be measured by slowly applying torque until the shear vane
414 began to rotate. The vane was preheated to lava temperature and inserted into the isothermal
415 core to avoid the effects of the cooler flow margins. To minimize the effects of shearing by
416 the cooler flow on the shaft, a ‘dummy end’ was used at each location. Additionally, the
417 measured torque required to initiate movement of the shaft at the same immersion depth
418 without the vane was subtracted from the torque with the vane attached. This instrument was
419 used at eight locations on two lava flows at different distances from the vent. The results
420 indicated that the yield strengths measured using the torque wrench were compatible with the
421 values obtained with the Mark 2 viscometer. Values increased from 6.05×10^2 Pa at 1083 °C,
422 close to the vent, to 1.4×10^3 Pa at 1080 °C, 7 m down flow and 2×10^3 Pa at 1070 °C, 24 m
423 down flow from the vent. These measurements demonstrate the potential to make systematic
424 measurements down an active flow.

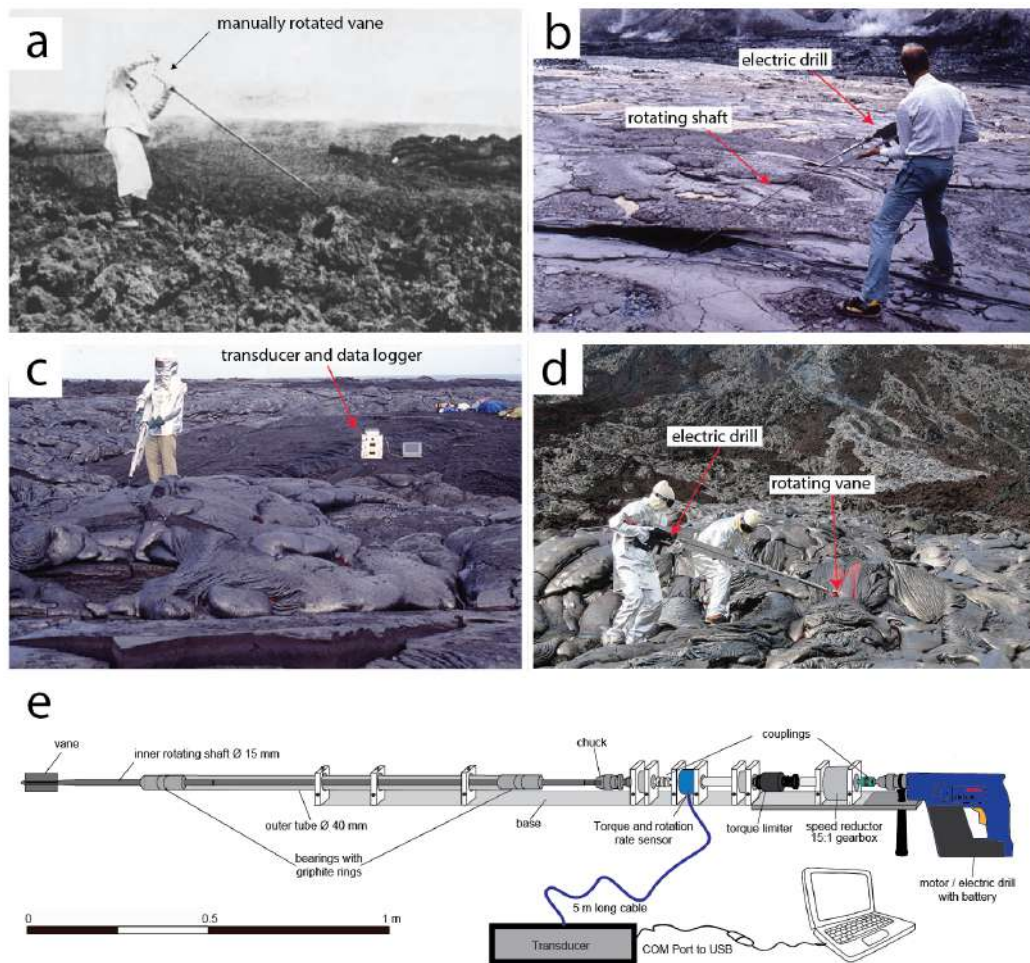
425 **3.6 Simple penetrometer employed at Klyuchevskoy, Russia, by Panov et al. (1988)**

426 During the 1983 Predskazannyi eruption at Klyuchevskoy volcano, Panov et al. (1988)
427 employed a simple penetrometer (Panov et al., 1985 in Russian, later translated into English
428 by Panov et al., 1988). The instrument was a steel pole, 14 mm in diameter and 2 m long,
429 with a rounded end. Viscosity was estimated from the measurement of the speed at which the
430 rod penetrated the lava under a known force and by assuming that the viscous drag was equal
431 to half of Stokes’ force (Eq. 5). In practice, the penetration speed was measured from the time
432 interval between the submersion of marks noted on the rod. The force acting on the rod was
433 the combined weight of the rod itself and the muscular effort applied. The rod was not pre-
434 heated, therefore when it was plunged into the lava a chilled margin formed around it. To
435 correct for this effect, Panov et al. (1988) added 1 to 2 mm to the rod diameter for the
436 calculation of viscosity. During measurements, the penetration rate did not change under
437 constant applied force, independently of the depth of penetration. The viscosity was measured
438 to be between 1.1×10^4 Pa s and 3.6×10^5 Pa s. No systematic variation was observed with
439 distance from the vent to the measurement location (15 to 35 m). Panov et al. (1988) noticed

440 the similarity (within an order of magnitude) of the penetrometer results with estimation of
441 viscosity obtained using the Jeffreys (1925) equation. No data on the lava chemistry and
442 crystal and bubble content was given.

443 **3.7 Vane rotated by hand to measure viscosity of Mount Etna 1983 lava flow by** 444 **Pinkerton and Norton (1995)**

445 Pinkerton and Norton (1995) presented results of viscosity measurements performed during
446 the eruption of Mount Etna in 1983. These viscosity measurements were performed using a
447 rotating vane system on a breakout from the main channel where the measured temperature
448 was 1095 °C. The vane was pre-heated and then inserted into the lava and rotated at different
449 rates by hand (Fig. 3a). The system was equipped with a torque meter to measure the torque
450 required to rotate the vane and rotation speeds were monitored with an optical tachometer.
451 Four data points were acquired before the lava began to develop an impenetrable crust. In
452 view of the limited range of rotation rate (5 – 9 rad/s), no unique rheological model could be
453 applied. Assuming Newtonian behavior, the viscosity was calculated to be 1.385×10^3 Pa s.
454 Applying a Bingham model, the yield strength was 3.7×10^2 Pa with a plastic viscosity of
455 1.26×10^3 Pa s and at unit strain rate the apparent viscosity is 1.63×10^3 Pa s. This range of
456 values was consistent with those measured in the laboratory on melted samples from the same
457 lava flow (Pinkerton and Norton, 1995, 1983). The lava was a trachy-basalt but unfortunately
458 crystal and bubble content was not given. However, field viscosity values are in close
459 agreement with those measured at the same temperature in the laboratory at for crystal content
460 between 30 and 40 vol. %.



461

462 **Figure 3:** Rotational viscometers: a) Pinkerton taking rheological measurements in 1983 at Mount Etna using a
463 manually rotated shear vane (Chester et al., 1986) ; b) Pinkerton in 1988 at Oldoinyo Lengai using the first motor-driven
464 shear vane (Pinkerton et al. 1995); c) Pinkerton et al. (1994) at Kilauea holding the new version of the motor-
465 driven rotational viscometer: d) Chevrel et al. (2018b) using the refurbished viscometer in 2016 at Kilauea. e)
466 Schematic representation of the refurbished viscometer, modified from Chevrel et al. (2018b)

467

468 3.8 Portable rotational viscometer to measure the viscosity of carbonatite at Oldoinyo 469 Lengai, Tanzania, by Pinkerton et al. (1995a)

470 Rheological field measurements performed in November 1988 on natrocarbonatite lavas at
471 Oldoinyo Lengai by Pinkerton et al. (1995) (Fig. 3b) were made using a motor-driven version
472 of the equipment used on Etna in 1983. A 24-V DC Bosch drill was used to drive a vane at
473 different, constant, rotation rates, which were measured using an optical tachometer. Torques
474 corresponding to different rotation rates were measured using a torque meter that was
475 mounted coaxially between the drive mechanism and the vane. This set of measurements
476 revealed that the vesicle-free natrocarbonatite lavas behaved as inelastic Newtonian fluids
477 with viscosities ranging from 1 to 5 Pa s. In contrast, highly vesicular lavas had apparent

478 viscosities of $0.7 - 1.2 \times 10^2$ Pa s at a strain rate of 1 s^{-1} and apparent viscosities of $0.3 - 3$ Pa
479 s at a strain rate of 3 s^{-1} . These measurements were slightly higher than those measured
480 subsequently in the laboratory by Norton and Pinkerton (1997) who concluded that these
481 differences arose from differences in vesicularity and volatile contents between laboratory
482 and field measurements.

483 **3.9 Portable rotational viscometer to measure the viscosity of pāhoehoe lobes at** 484 **Kilauea, Hawaii, by Pinkerton et al. (1995b)**

485 Pinkerton (1994) and Pinkerton et al. (1995b) performed rheological measurements on small
486 pāhoehoe lobes erupted at Kilauea in September 1994 using a new rotational portable
487 viscometer based on the prototype employed at Oldoinyo Lengai. The viscometer was driven
488 by a 24-V DC Bosch drill motor connected to a (15:1) reduction gearbox, a torque limiter and
489 a torque-rotation rate sensor (Fig 3c). The sensor (DORT Optical rotary torque transducer
490 from Sensor Technology Ltd) was linked via a transducer to a data logger. After each set of
491 measurements, raw rotation rate and torque data were downloaded to a laptop and later
492 processed with custom software. The main drive shaft was protected from the cooler outer
493 layer of the flow by an outer tube with bearing assemblies (containing graphite rings to
494 minimize friction) at regular intervals. This helped to maintain alignment of the inner shaft.
495 Three pāhoehoe lobes (20 to 50 cm thick) were measured, each of which had maximum
496 internal temperatures of $1146 \text{ }^\circ\text{C}$. All lavas measured had properties that could be
497 approximated by a pseudoplastic power law model with plastic viscosity ranging from 2.3 to
498 5.5×10^2 Pa s and with corresponding power law exponents of 0.77 and 0.53, respectively.
499 Pinkerton et al. (1995b) concluded that the higher viscosities resulted from lava with higher
500 crystallinity and bubble content, but quenched samples collected following each measurement
501 were not analyzed until the present study when one sample was analyzed (see appendix). The
502 lava can be classified as porphyritic basalt with 4 vol.% of olivine phenocrysts and 12 vol.%
503 of microlites (olivine + plagioclase + clinopyroxene) within a glassy matrix (55.1 wt. % SiO_2
504 and Mg # = 48). The vesicle content was measured at 34 vol. % from image analyses and
505 from density-derived measurements. The viscosity of the interstitial liquid was calculated
506 from the glass composition (including 0.07 wt. % H_2O) using the model of Giordano et al.
507 (2008) at $1146 \text{ }^\circ\text{C}$. The effect of crystals and of bubbles on viscosity was estimated following
508 the methods of Mader et al. (2013) and Llewellyn and Manga (2005), respectively.
509 Considering deformable bubbles (capillary number >1 for the strain rates applied during the
510 measurements), the viscosity is estimated at 3.5×10^2 Pa s, which is in agreement with the

511 field measurements at unit strain rate. Unfortunately no other sample could be analyzed to
512 examine whether from one lobe to another the texture was different so as to explain the range
513 of viscosities measured.

514 **3.10 Viscometry using a simple penetrometer on pāhoehoe lobes at Tolbachik, Russia,** 515 **by Belousov and Belousova (2018)**

516 In 2013, during the Tolbachik eruption, Belousov and Belousova (2018) performed viscosity
517 measurements on several pāhoehoe lobes using a simple penetrometer (Fig. 1c) based on the
518 method of Panov et al. (1985). In these experiments, Belousov and Belousova measured
519 penetration rate of the rod as it passed through the pāhoehoe lobe producing a viscosity
520 profile from the lobe top to the base (a distance of 10 to 25 cm). The speed of penetration was
521 measured via video footage where marks on the penetrometer were tracked on each frame.
522 The force of penetration was applied manually and recorded using a spring balance. Repeated
523 measurements on each lobe and/or neighboring lobes (about 20 in total) gave interior
524 viscosities between 5×10^3 and 5×10^4 Pa s. The viscosity of the upper and basal section of
525 the lobes was measured as high as 6×10^4 to 4×10^5 Pa s. Measurements performed at
526 various distances from the vent resulted in constant viscosity. The 'a'ā flow type could not be
527 measured because of the impenetrable crust. Where the measurements were performed,
528 maximum temperatures of 1082 °C were recorded with a K-type thermocouple at depths of
529 several centimeters. The authors did not sample the lava at the moment of the measurements,
530 but reported the chemical and textural analyses of previous studies. The lava was sub-aphyric
531 basaltic trachyandesite (52 wt. % SiO₂) with 25 to 43 vol.% of crystals (mainly plagioclase
532 and olivine) and 6 vol.% of vesicles (Plechov et al., 2015). Plechov et al. (2015) estimated the
533 lava viscosity at $0.9 - 2.8 \times 10^3$ Pa s from chemical and textural characteristics. They used the
534 model of Bottinga and Weill (1970) at 1100 °C for the melt viscosity and the Einstein-Roscoe
535 model for the effect of crystals. As noted by Belousov and Belousova (2018), this estimate is
536 in good agreement with their field viscosity measurements of the most fluid part of the
537 pāhoehoe lobes. Recently, Ramsey et al. (2019) also estimated the viscosity from textural and
538 chemical data given by Plechov et al. (2015) but using Giordano et al. (2008) for the
539 interstitial melt viscosity at 1082°C. This revealed a slightly higher viscosity of 1.9×10^4 Pa s,
540 which is in better agreement with the Belousov and Belousova (2018) measurements.

541 **3.11 Portable rotational viscometer to measure the viscosity of pāhoehoe lobes of the**
542 **61G lava flow at Kilauea, Hawaii by Chevrel et al. (2018b)**

543 In 2016, Chevrel et al. (2018a) used the same instrument as Pinkerton et al. (1995b) but it
544 was refurbished and equipped with a different torque sensor (TORQSENSE E300 from
545 Sensor Technology Ltd), communication system and new vanes. Tests in the laboratory using
546 a calibrated viscosity standard, showed that the instrument could measure absolute viscosity
547 with less than 5 % error, but was limited to strain-rates $> 0.6 \text{ s}^{-1}$ and torque measurements
548 above $3 \times 10^2 \text{ Pa}$. Chevrel et al. carried out measurements on pāhoehoe lobes from the 61G
549 lava flow of Kilauea's Pu'u 'Ō'ō eruption (Fig. 3d). A Newtonian viscosity of $3.8 \times 10^2 \text{ Pa s}$
550 was measured for strain-rates $> 1 \text{ s}^{-1}$ and at 1144 °C . No yield strength was measured
551 indicating that yield strength, if present, must be below the 300 Pa measurement limit of the
552 device. In contrast to Pinkerton et al. (1995b), low strain rates could not be measured (due to
553 torque sensor sensitivity). The data could be fitted with a power law model of the form
554 $\tau = 424 \dot{\gamma}^{0.88}$ but with a low fit coefficient of 0.79. Chevrel et al. also collected samples by
555 quenching the lava attached to the share vane and completed textural and petrographic
556 analyses, which allowed quantification of the effect of each phase on viscosity. The viscosity
557 of the interstitial liquid was calculated from the glass composition (including 0.07 wt. % H_2O)
558 using the model of Giordano et al. (2008). The effect of crystals (16 vol. %) and of bubbles
559 (50 vol. %) on viscosity was estimated following the methods of Mader et al. (2013) and
560 Llewellyn and Manga (2005), respectively. Considering deformable bubbles (capillary number
561 was calculated > 1), the results gave a viscosity of $2.2 \times 10^2 \text{ Pa s}$, in agreement with the field
562 measurements. Considering the bubbles to be rigid spheres resulted in an overestimation of
563 the viscosity by one-to-two orders of magnitude.

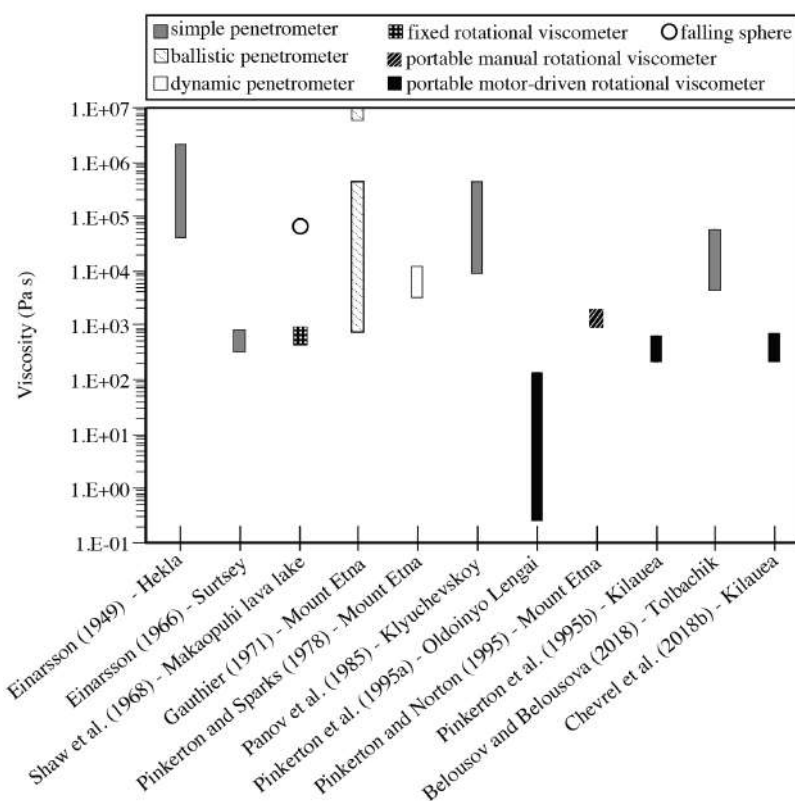
564 **4 Discussion**

565 **4.1 Field viscometers**

566 Penetrometers have been employed to measure lava's rheological properties from the
567 first published measurement by Einarsson (1948) until recently (Belousov and Belousova,
568 2018). This instrument has been favored because it is light, easy to build (it consists of a rod
569 equipped with a dynamometric gauge) and permits quick estimates of the lava viscosity
570 within a wide range ($10^3 - 10^6 \text{ Pa s}$; Figure 4). However, as highlighted by Einarsson (1966),
571 the penetrometer is not well adapted for low viscosity lava ($< 10^3 \text{ Pa s}$) because it sinks too

572 rapidly into the lava. Additionally, simple penetrometers do not allow rheological flow curves
573 to be calculated because strain rate cannot be varied at the same position (viscosity is
574 estimated from penetration velocity). Furthermore, unless the rod has been pre-heated, or
575 meticulous calibration has been performed with similar condition as in the field (i.e., with a
576 gradient of viscosity due to cooler outer surface), the measurements are often biased by the
577 outer cooler surface of the lava. More sophisticated penetrometers such as the Mark 2
578 employed by Pinkerton and Sparks (1978) can prevent the effect of the cooler lava surface.

579 A falling sphere method was employed by Shaw et al. (1968), and although he obtained
580 a measurement at a low strain rate (0.004 s^{-1}), this method can only be employed on a stable
581 lava lake of sufficient depth, and with a suitable thick crust. Nonetheless this is currently the
582 only way to measure the viscosity of silicate liquids under pressure in the laboratory (Kono,
583 2018).



584
585 **Figure 4:** Viscosity range measured during field campaigns. The boxes are grey-shaded according to the type of
586 viscometers.

587
588 Rotational viscometry appears to be the most promising approach for field
589 measurement on low viscosity lava ($< 10^4 \text{ Pa s}$; Figure 4). This instrument can apply various
590 strain rates ($0.1 - > 5 \text{ s}^{-1}$; Figure 4) that permit the construction of full flow curves (Pinkerton

591 and Norton, 1995; Pinkerton et al.1995b). In 1968, the rotational viscometer set up by Shaw
592 et al. (1968) provided accurate measurements. However it is unsuitable for active lava flows
593 that are in constant motion and often have short-lived instable levées. In 1994, Pinkerton
594 (1994) built the first generation of portable, motor-driven, rotational viscometer. The
595 measurements presented in Chevrel et al. (2018a) showed that this instrument, equipped with
596 a new torque sensor communication system, continues to work well, but has some important
597 limitations. These are 1) it was not possible to achieve low strain rate ($< 1 \text{ s}^{-1}$) because of
598 limiting low rotation speeds and 2) this instrument is bulky and heavy ($>15 \text{ kg}$) and requires
599 two people to handle it and a third person to monitor the results, which hinders the easy, fast
600 and flexible handling required in the field around an active lava.

601 We suggest that a combination of two instruments, a rotational viscometer for low
602 viscosity range ($< 10^4 \text{ Pa s}$) and a dynamic penetrometer for higher viscosities ($10^3 - 10^6 \text{ Pa}$
603 s), may therefore be the most appropriate procedure. For lavas with higher viscosity ($> 10^6 \text{ Pa}$
604 s) no field instruments are available for such measurement. Besides, field viscometry will be
605 extremely challenging because such flows are usually ‘a’ā to blocky with an outer thick
606 fragmented crust that is impossible to approach and penetrate. In addition, the time required to
607 measure viscosity may expose the operator to unacceptable risk from falling blocks.

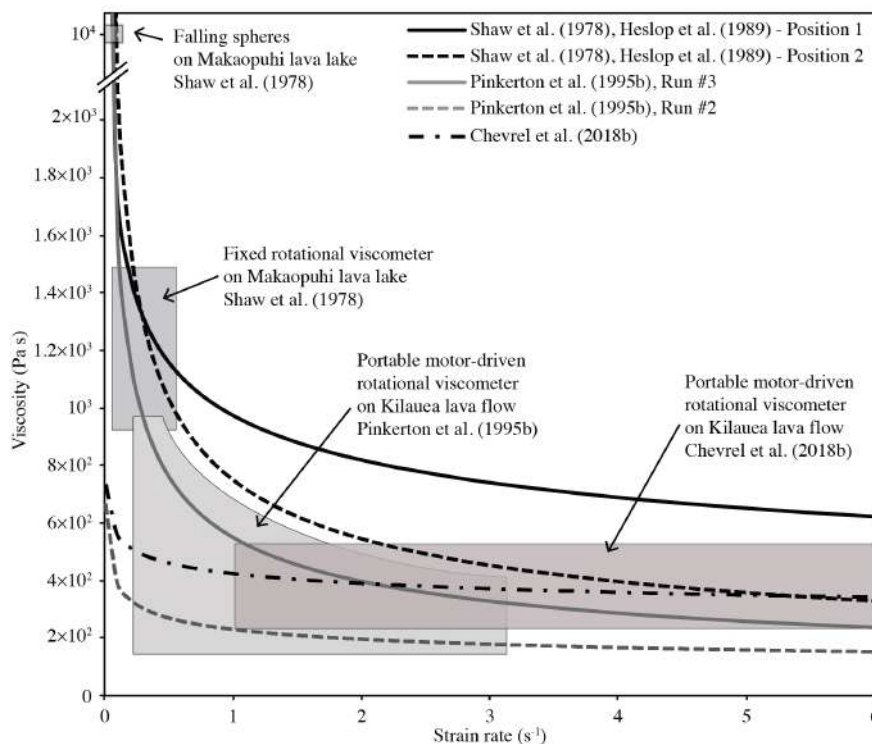
608

609 **4.2 Comparison of the rheological results in different geological settings**

610 **4.2.1 Hawaiian lavas**

611 Using rotational viscometers, the viscosity of Hawaiian lavas measured in the field at
612 temperatures between $1146 \text{ }^\circ\text{C}$ and $1130 \text{ }^\circ\text{C}$, falls within the range $1.5 \times 10^3 \text{ Pa s}$ at strain
613 rates less than 1 s^{-1} to $2.6 \times 10^2 \text{ Pa}$ at strain rates higher than 1 s^{-1} (Figure 5). The
614 measurements of Shaw et al. (1968) were performed at low strain rate ($0.1 - 1 \text{ s}^{-1}$), and
615 although the data were first fitted with a Bingham model, later Heslop et al. (1989) showed
616 that a power law model would be more appropriate. Pinkerton et al. (1995) applied low-to-
617 moderate strain rates ($0.2 - 3.2 \text{ s}^{-1}$) that also showed the pseudo-plastic behavior of the lava.
618 In contrast, Chevrel et al. (2018a) performed measurements at higher strain rates ($>1 \text{ s}^{-1}$) and
619 although they could be fitted with a power law, the Newtonian rheological model provided a
620 better fit at $3.8 \times 10^2 \text{ Pa s}$. The similarity between the collected samples and the viscosities
621 obtained at unit strain rate in 1994 and 2016, using almost the same instrument but 22 years
622 apart, is consistent with the fact that temperature, composition and texture (amount of bubbles
623 and crystals) was similar in the two field studies. These viscosities are lower than the values

624 obtained by Shaw et al. (1968), which is consistent with a higher temperature, lower crystal
625 content and higher content of deformable bubble in the lava from Pinkerton et al. (1995) and
626 Chevrel et al. (2018b). The value obtained by Shaw et al. (1968) using a falling sphere
627 revealed even higher viscosities ($> 10^4$ Pa s) at very low strain rates (0.004 s $^{-1}$). All three data
628 sets suggest a pseudo-plastic behavior of Hawaiian lavas under these conditions (Figure 5).



629
630 **Figure 5:** Variation of viscosity with strain rate for Hawaiian lavas as obtained from field viscometry. Boxes
631 represent the measured range of viscosity and strain rate and curves are best fits as given by the different
632 studies.

633
634 Among these field experiments at Hawaii, none have directly recorded a yield
635 strength. The estimation of yield strength given by Shaw et al. (1968) was made by fitting the
636 data to a Bingham model. According to laboratory experiments of Hawaiian lavas at
637 subliquidus condition (Ryerson et al. 1988; Sehlke et al., 2014), yield strength may appear
638 with crystallization but should be less than 200 Pa for the crystal content of the lavas
639 measured in the field (< 25 vol. %). Unfortunately, this relatively low yield strength is, to
640 date, difficult, if not impossible, to measure using current field instruments. Further
641 measurements at low shear stresses and low strain rates are needed to determine whether yield

642 strength can develop. Until then a power law model is considered to be the most appropriate
643 model to characterize the behavior of Hawaiian lava at temperatures above 1130 °C (Figure
644 5).

645 The agreement between field measurements and the model-based viscosity using
646 textural and chemical characterization shows our capacity of estimating and measuring three-
647 phase mixture viscosity. However, this is only true for a given temperature and only when an
648 exhaustive sample analyses is generated. Further measurements on pāhoehoe lava need to be
649 performed so as to test the sensitivity of viscosity to the effect small thermal, physical of
650 chemical changes within a lava field.

651 **4.2.2 Etnean lavas**

652 At Mount Etna, measurements were performed on ‘a‘ā type lava flows using different
653 instruments including penetrometers and a manually-operated rotating viscometer (Figure 4).
654 The measured viscosities (either on lava blocks or on channelized lava) range mostly between
655 10^3 Pa s and 10^4 Pa s. Gauthier (1973) recorded very high viscosities ($> 10^7$ Pa s) using a
656 ballistic penetrometer but these high values are unduly influenced by the cooler outer crust
657 (penetration depth was only 1 cm) and therefore do not represent the flowing lava interior.
658 The viscosities measured by Pinkerton and Sparks (1978) using the Mark 2 penetrometer
659 were higher (9.4×10^3 Pa s) than those measured by Pinkerton and Norton (1995) using a
660 rotational viscometer (approx. 1.3×10^3 Pa s). This difference is considered to be a result of a
661 combination of factors, including different eruptive temperatures (1086 °C in 1975 compared
662 with 1095 °C in 1983), different crystal content (45 vol. % in 1975 and < 40 vol. % 1983),
663 and lower strain rates used in 1975 ($0 - 0.15$ s⁻¹) compared with 1983 ($0.7 - 1.4$ s⁻¹).
664 Pinkerton and Sparks (1978) measured lava yield strength using various instruments and they
665 found a clear correlation with temperature and consequently crystallinity.

666 Although the rheological properties of Etnean lavas are now well constrained from
667 laboratory experiments (e.g. Pinkerton and Norton, 1995; Vona et al., 2011; Vona and
668 Romano, 2013), there are not enough field measurements to build flow curves under field
669 conditions.

670 **4.2.3 Kamchatka and Icelandic lavas**

671 The measurements on basaltic-andesite lavas from Klyuchevskoy and Tolbachik
672 showed that the pāhoehoe lobes measured by Belousov and Belousova (2018) have slightly
673 lower viscosities than the ‘a‘ā flow measured by Panov et al. (1988): $0.5 - 5 \times 10^4$ Pa s and
674 $0.11 - 3.6 \times 10^5$ Pa s, respectively. However, the investigation by Belousov and Belousova

675 (2018) at Tolbachik, revealed that the lava traveling within the ‘a‘ā channel was slightly less
676 viscous than the early erupted pāhoehoe lava. This is consistent with some observations at
677 Hawaii, where pāhoehoe flows formed from the rupture of ‘a‘ā front flow (Hon et al., 2003).
678 In general the Kamchatka pāhoehoe lobes are more viscous than Hawaiian lavas, which is
679 attributed to the lower temperature, higher silica content and higher crystallinity of the former
680 in comparison to the later.

681 Finally, Einarsson (1949; 1966) measured viscosities at Surtsey as low as 5×10^2 Pa s
682 and up to 1.5×10^6 Pa s at Hekla both using the same penetrometer. However the value at
683 Surtsey was challenging to measure, as the rod sank too quickly under its own weight.
684 Unfortunately, there are no other field measurements to compare with. This highlights the
685 need for more data to build flow curves and determine the lava rheological behavior from
686 these field locations in Russia and Iceland.

687 **4.3 Future requirements for field viscometry**

688 Reducing errors associated with field measurements requires accurate sensors as well
689 as meticulous setup and calibration, which is difficult to achieve in the field where conditions
690 are more complex than in the lab. Field measurements are always constrained by the lava’s
691 thermal dynamics. To reduce the effects of crust formation during measurements the
692 instrument needs to be pre-heated and inserted into fresh molten lava, emerging through
693 breaches in the crust, or at the breaking point of pāhoehoe lobes, where little-to-no crust is
694 present. The time of the measurements then needs to be always shorter than crust formation.
695 Another procedure to minimize the effect of crust formation is to use viscometers like the
696 “Mark 2” (Pinkerton and Sparks, 1978), which allow triggering the sensor once the lava
697 isothermal core is reached. A detailed engineering drawing of the Mark 2 can be found in
698 Pinkerton (1978; Figure 2). Note also that interpretation of the results is non-trivial, but pre-
699 and post- calibration in fluids of different viscosity can be used to validate the results from an
700 analysis of the raw data. Gauthier (1971) proposed a set up similar in sophistication to that
701 used in the laboratory, where the viscometer head would float on the lava surface, protected
702 from radiant heat by a cooling carapace. This would drive a sensitive spindle plunged in the
703 lava. Although this instrument may produce useful data, it would be time-consuming and
704 expensive to build, and there would be a high risk of losing it during utilization in the field.

705 Future viscometers need to be robust, light enough to be carried over rough ground to
706 remote locations, easily mounted and easy to handle, ideally by one person. Additionally, in
707 order to capture the full rheological behavior of lava, viscometers need to apply low strain

708 rates ($< 1 \text{ s}^{-1}$) and record low shear stresses ($< 200 \text{ Pa}$). This will constrain the dimensions of
709 the shear vane or spindle, torque sensor capability and motor power. Using newer
710 (electronically controlled) technology and a lighter and modern motorized system, a new
711 generation of rotational viscometer seems to be the most suitable way forwards toward future
712 measurements on basaltic lava.

713 The material used for field viscometer needs to be resistant to high temperatures. In
714 the laboratory, crucibles containing the lava and rotating spindles are usually made of
715 platinum-rhodium alloy or alumina ceramics. However, at the torques applied in the field, the
716 former does not supply sufficient mechanical strength and may, therefore, deform too easily
717 and the latter may break. Instead low carbon stainless steel alloy is often favored. This
718 material is resistant both mechanically and to heat and seems to have the best value for
719 money. Although its composition (of mainly iron) may contaminate the lava, the degree of
720 contamination is considered to be insignificant considering the timescale of the
721 measurements, although this should be investigated in detail during future experiments.

722 Finally, and most importantly, viscosity measurements must be made in combination
723 with temperature measurements and lava sampling for textural analysis. The rheological
724 evolution of lava during flow is controlled by the cooling rate (Giordano et al., 2007), which
725 also controlled the crystal size distribution (Vetere et al., 2015). Recent laboratory-based
726 work has shown that viscometry associated with synchronous temperature measurement is the
727 key for understanding lava flow behavior at conditions pertinent to nature (Kolzenburg et al.,
728 2017, 2016). This also includes changes in shear rate and oxygen fugacity (Kolzenburg et al.,
729 2018a, 2018b). Future field viscometers should therefore incorporate a thermocouple.

730 Textural and petrographic analysis of the sample is the key to understanding how
731 crystal and bubble content affect rheology during lava emplacement. The molten lava must
732 always be sampled and quenched rapidly to conserve the texture at the location of the
733 viscosity measurement. Future field campaigns should focus on measuring lava properties,
734 temperature and lava texture as a function of distance from the vent to the front and across the
735 flow, in order to map lava rheology in 4D through the flow.

736 **5 Conclusion**

737 Field viscometry at active lava flows is the only way to capture the rheology of lava in its
738 natural state. It is also a very challenging method to employ in the field. Since the 1940's
739 there are eleven studies. These field experiments and their results highlight that they have

740 considerable potential, but the definitive study has yet to be undertaken. The most important
741 aspect is the choice and design of the viscometer. The rotational viscometer seems to be the
742 most appropriate instrument for low viscosity lava ($< 10^4 - 10^5$ Pa s) as it allows a large range
743 of strain rate to be applied (0.1 to > 5 s⁻¹). For higher viscosity lava ($10^5 - 10^6$ Pa s), well-
744 calibrated penetrometers designed to avoid the effects of the cooler outer lava surface are
745 suitable. Above 10^6 Pa s measurement is not viable, as penetration becomes impossible.
746 Using field measurements, flow curves could be established only for Hawaiian lavas and
747 revealed a pseudo-plastic behavior. Further works still remain to be carried out on other
748 basaltic volcanoes to ensure a full understanding of the lava rheological behavior under field
749 conditions.

750 If suitable precautions are taken during measurements and post-processing of data,
751 field viscometry in combination with simultaneous temperature measurements and laboratory
752 studies of quenched samples collected at each measurement site will improve our
753 understanding of evolving lava viscosity as a function of cooling rate, degassing and
754 crystallisation. This will create the data required for the development of flow emplacement
755 models. Future improvements include adding thermal sensors and building lighter and
756 electronically controlled viscometers with simple operating systems that can achieve a wide
757 range of strain- and stress-rates.

758

759 **Acknowledgement**

760 We warmly acknowledge M. R. James for useful discussions and for assisting with equipment
761 refinement. We acknowledge S. Kolzenburg for thorough reviews and Gillian R. Foulger for
762 handling the manuscript. This research was partly financed by the Auvergne fellowship
763 (Labex ClerVolc) attributed to M.O.Chevrel and by the Agence National de la Recherche
764 through the project LAVA (Program: DS0902 2016; Project: ANR-16 CE39-0009,
765 <http://www.agence-nationale-recherche.fr/Projet-ANR-16-CE39-0009>). This is ANR-LAVA
766 contribution no. 10 and ClerVolc publication n°349.

767

768

769 **References**

770 Avard, G., Whittington, A.G., 2012. Rheology of arc dacite lavas: experimental determination
771 at low strain rates. *Bull. Volcanol.* 74, 1039–1056. [https://doi.org/10.1007/s00445-012-](https://doi.org/10.1007/s00445-012-0584-2)
772 0584-2

- 773 Bagdassarov, N.S., Dingwell, D.B., 1993. Deformation of foamed rhyolites under internal and
774 external stresses: An experimental investigation. *Bulletin Volcanol.* 55, 147–154.
775 <https://doi.org/10.1007/BF00301512>
- 776 Bagdassarov, N.S., Dingwell, D.B., 1992. A rheological investigation of vesicular rhyolite. *J.*
777 *Volcanol. Geotherm. Res.* 50, 307–322. [https://doi.org/10.1016/0377-0273\(92\)90099-Y](https://doi.org/10.1016/0377-0273(92)90099-Y)
- 778 Bagdassarov, N.S., Dingwell, D.B., Webb, S.L., 1994. Viscoelasticity of crystal-bearing and
779 bubble-bearing rhyolite melts. *Phys. Earth Planet. Inter.* 83.
780 [https://doi.org/10.1016/0031-9201\(94\)90066-3](https://doi.org/10.1016/0031-9201(94)90066-3)
- 781 Bagdassarov, N.S., Pinkerton, H., 2004. Transient phenomena in vesicular lava flows based
782 on laboratory experiments with analogue materials. *J. Volcanol. Geotherm. Res.* 132,
783 115–136.
- 784 Balmforth, N.J., Craster, R. V., Rust, A.C., Sassi, R., 2007. Viscoplastic flow over an inclined
785 surface. *J. Nonnewton. Fluid Mech.* 142, 219–243.
786 <https://doi.org/10.1016/j.jnnfm.2006.07.013>
- 787 Barnes, H.A., 1989. *An Introduction to Rheology*, Rheology series 3. U.S. and Canada,
788 Elsevier Science.
- 789 Belousov, A., Belousova, M., 2018. Dynamics and viscosity of ‘a’ā and pāhoehoe lava flows
790 of the 2012-2013 eruption of Tolbachik volcano, Kamchatka (Russia). *Bull. Volcanol.*
791 80. <https://doi.org/doi.org/10.1007/s00445-017-1180-2>
- 792 Bilotta, G., Herault, A., Cappello, A., Ganci, G., Negro, C. Del, 2014. GPUSPH: a Smoothed
793 Particle Hydrodynamics model for the thermal and rheological evolution of lava flows,
794 in: Harris, A.J.L., De Groeve, T., Garel, F., Carn, S.A. (Eds.), *Detecting, Modelling and*
795 *Responding to Effusive Eruptions*. Geological Society, London, pp. 387–408.
796 <https://doi.org/10.1144/SP426.24>
- 797 Bottinga, Y., Weill, D.F., 1972. The viscosity of magmatic silicate liquids: A model for
798 calculation. *Am. J. Sci.* 272, 438–475. <https://doi.org/10.2475/ajs.272.5.438>
- 799 Bottinga, Y., Weill, D.F., 1970. Density of liquid silicate systems calculated from partial
800 molar volumes of oxide components. *Am. J. Sci.* 269(2), 169.
801 <https://doi.org/10.2475/ajs.269.2.169>
- 802 Caricchi, L., Giordano, D., Burlini, L., Ulmer, P., 2008. Rheological properties of magma
803 from the 1538 eruption of Monte Nuovo (Phlegrean Fields, Italy): An experimental
804 study. *Chem. Geol.* 256, 158–171. <https://doi.org/10.1016/j.chemgeo.2008.06.035>
- 805 Cashman, K. V, Thornber, C., Kauahikaua, J.P., 1999. Cooling and crystallization of lava in

- 806 open channels, and the transition of pāhoehoe lava to ‘a‘ā. *Bull. Volcanol.* 61, 306–323.
807 <https://doi.org/https://doi.org/10.1007/s004450050299>
- 808 Castruccio, A., Contreras, M.A., 2016. The influence of effusion rate and rheology on lava
809 flow dynamics and morphology: A case study from the 1971 and 1988-1990 eruptions at
810 Villarrica and Lonquimay volcanoes, Southern Andes of Chile. *J. Volcanol. Geotherm.*
811 *Res.* 327, 469–483. <https://doi.org/10.1016/j.jvolgeores.2016.09.015>
- 812 Castruccio, A., Rust, A.C., Sparks, R.S.J., 2013. Evolution of crust- and core-dominated lava
813 flows using scaling analysis. *Bull. Volcanol.* 75, 681. [https://doi.org/10.1007/s00445-](https://doi.org/10.1007/s00445-012-0681-2)
814 [012-0681-2](https://doi.org/10.1007/s00445-012-0681-2)
- 815 Castruccio, A., Rust, A.C., Sparks, R.S.J., 2010. Rheology and flow of crystal-bearing lavas:
816 Insights from analogue gravity currents. *Earth Planet. Sci. Lett.* 297, 471–480.
817 <https://doi.org/10.1016/j.epsl.2010.06.051>
- 818 Champallier, R., Bystricky, M., Arbaret, L., 2008. Experimental investigation of magma
819 rheology at 300 MPa: From pure hydrous melt to 76 vol.% of crystals. *Earth Planet. Sci.*
820 *Lett.* 267, 571–583. <https://doi.org/10.1016/j.epsl.2007.11.065>
- 821 Chester, D.K., Duncan, A.M., Guest, J.E., Kilburn, C.R.J., 1986. Mount Etna: The anatomy of
822 a volcano. Springer Netherlands. <https://doi.org/10.1007/978-94-009-4079-6>
- 823 Chevrel, M.O., Cimarelli, C., DeBiasi, L., Hanson, J.B., Lavallée, Y., Arzilli, F., Dingwell,
824 D.B., 2015. Viscosity measurements of crystallizing andesite from Tungurahua volcano
825 (Ecuador). *Geochemistry, Geophys. Geosystems* 16, 870–889.
826 <https://doi.org/10.1002/2014GC005661>
- 827 Chevrel, M.O., Guilbaud, M.-N., Siebe, C., 2016. The ~AD 1250 effusive eruption of El
828 Metate shield volcano (Michoacán, Mexico): Magma source, crustal storage, eruptive
829 dynamics, and lava rheology. *Bull. Volcanol.* 78, 1–28. [https://doi.org/10.1007/s00445-](https://doi.org/10.1007/s00445-016-1020-9)
830 [016-1020-9](https://doi.org/10.1007/s00445-016-1020-9)
- 831 Chevrel, M.O., Harris, A.J.L., James, M.R., Calabrò, L., Gurioli, L., Pinkerton, H., 2018b.
832 The viscosity of pāhoehoe lava: In situ syn-eruptive measurements from Kilauea,
833 Hawaii. *Earth Planet. Sci. Lett.* 493, 161–171. <https://doi.org/10.1016/j.epsl.2018.04.028>
- 834 Chevrel, M.O., Labroquere, J., Harris, A.J.L., Rowland, S.K., 2018a. PyFLOWGO: an open-
835 source platform for simulation of channelized lava thermo-rheological properties.
836 *Comput. Geosci.* 111, 167–180. <https://doi.org/10.1016/j.cageo.2017.11.009>
- 837 Chevrel, M.O., Platz, T., Hauber, E., Baratoux, D., Lavallée, Y., Dingwell, D.B., 2013. Lava
838 flow rheology: A comparison of morphological and petrological methods. *Earth Planet.*

- 839 Sci. Lett. 384, 102–120. <https://doi.org/10.1016/j.epsl.2013.09.022>
- 840 Cigolini, C., Borgia, A., Casertano, L., 1984. Intra-crater activity, ‘a‘ā-block lava, viscosity
841 and flow dynamics: Arenal Volcano, Costa Rica. *J. Volcanol. Geotherm. Res.* 20, 155–
842 176. [https://doi.org/10.1016/0377-0273\(84\)90072-6](https://doi.org/10.1016/0377-0273(84)90072-6)
- 843 Cimarelli, C., Costa, A., Mueller, S., Mader, H.M., 2011. Rheology of magmas with bimodal
844 crystal size and shape distributions: Insights from analog experiments. *Geochem.*
845 *Geophys. Geosyst.* 12, Q07024. <https://doi.org/10.1029/2011GC003606>
- 846 Coppola, D., Laiolo, M., Franchi, A., Massimetti, F., Cigolini, C., Lara, L.E., 2017.
847 Measuring effusion rates of obsidian lava flows by means of satellite thermal data. *J.*
848 *Volcanol. Geotherm. Res.* 347, 82–90. <https://doi.org/10.1016/j.jvolgeores.2017.09.003>
- 849 Cordonnier, B., Hess, K.U., Lavalle, Y., Dingwell, D.B., 2009. Rheological properties of
850 dome lavas: Case study of Unzen volcano. *Earth Planet. Sci. Lett.* 279, 263–272.
851 <https://doi.org/10.1016/j.epsl.2009.01.014>
- 852 Costa, A., Caricchi, L., Bagdassarov, N.S., 2009. A model for the rheology of particle-bearing
853 suspensions and partially molten rocks. *Geochemistry Geophys. Geosystems* 10,
854 Q03010. <https://doi.org/10.1029/2008GC002138>
- 855 Crisci, G.M., Di Gregorio, S., Pindaro, O., Ranieri, G.A., 1986. Lava flow simulation by a
856 discrete cellular model: first implementation. *Int. J. Model. Simul.* 6, 137–140.
- 857 Crisp, J., Cashman, K. v., Bonini, J.A., Hougen, S.B., Pieri, D.C., 1994. Crystallization
858 history of the 1984 Mauna Loa lava flow. *J. Geophys. Res.* 99, 7177–7198.
859 <https://doi.org/10.1029/93JB02973>
- 860 Dingwell, D.B., 1986. Viscosity-temperature relationships in the system Na₂Si₂O₅-
861 Na₄Al₂O₅. *Geochim. Cosmochim. Acta* 50, 1261–1265.
- 862 Einarsson, T., 1966. Studies of temperature, viscosity, density and some types of materials
863 produced in the Surtsey eruption, Surtsey Research Program Report.
- 864 Einarsson, T., 1949. The flowing lava. Studies of its main physical and chemical properties.,
865 in: *The Eruption of Hekla 1947-1948*. Soc Scientiarum Islandica, Reykjavik, pp. 1–70.
- 866 Einstein, A., 1906. Eine neue Bestimmung der Molekuldimensionen. *Ann. Phys.* 19, 289.
- 867 Fink, J.H., Zimbelman, J.R., 1986. Rheology of the 1983 Royal Gardens basalt flows, Kilauea
868 Volcano, Hawaii. *Bull. Volcanol.* 48, 87–96. <https://doi.org/10.1007/BF01046544>
- 869 Ganci, G., Vicari, A., Cappello, A., Del Negro, C., 2012. An emergent strategy for volcano
870 hazard assessment: From thermal satellite monitoring to lava flow modeling. *Remote*
871 *Sens. Environ.* 119, 197–207. <https://doi.org/10.1016/j.rse.2011.12.021>

- 872 Gauthier, F., 1973. Field and laboratory studies of the rheology of Mount Etna lava. *Philos.*
873 *Trans. R. Soc. London A Math. Phys. Eng. Sci.* 274, 83–98.
- 874 Gauthier, F., 1971. Etude comparative des caractéristiques rhéologiques des laves basaltiques
875 en laboratoire et sur le terrain. PhD, Univ. Paris-Sud, Fac. des Sci. d'Orsay.
- 876 Giordano, D., Dingwell, D.B., 2003. Non-Arrhenian multicomponent melt viscosity: a model.
877 *Earth Planet. Sci. Lett.* 6556, 1–13. [https://doi.org/10.1016/S0012-821X\(03\)00042-6](https://doi.org/10.1016/S0012-821X(03)00042-6)
- 878 Giordano, D., Polacci, M., Longo, A., Papale, P., Dingwell, D.B., Boschi, E., Kasereka, M.,
879 2007. Thermo-rheological magma control on the impact of highly fluid lava flows at Mt.
880 Nyiragongo. *Geophys. Res. Lett.* 34.
- 881 Giordano, D., Russell, J.K., Dingwell, D.B., 2008. Viscosity of magmatic liquids: A model.
882 *Earth Planet. Sci. Lett.* 271, 123–134. <https://doi.org/10.1016/j.epsl.2008.03.038>
- 883 Griffiths, R.W., 2000. The Dynamics of Lava Flows. *Annu. Rev. Fluid Mech.* 32, 377–518.
884 <https://doi.org/10.1146/annurev.fluid.32.1.477>
- 885 Guilbaud, M.N., Blake, S., Thordarson, T., Self, S., 2007. Role of Syn-eruptive Cooling and
886 Degassing on Textures of Lavas from the ad 1783-1784 Laki Eruption, South Iceland. *J.*
887 *Petrol.* 48, 1265–1294. <https://doi.org/10.1093/petrology/egm017>
- 888 Harris, A.J.L., Allen, J.S., 2008. One-, two- and three-phase viscosity treatments for basaltic
889 lava flows. *J. Geophys. Res.* 113, B09212. <https://doi.org/10.1029/2007JB005035>
- 890 Harris, A.J.L., Bailey, J., Calvari, S., Dehn, J., 2005. Heat loss measured at a lava channel and
891 its implications for down-channel cooling and rheology. *Geol. Soc. Am. Spec. Pap.* 396,
892 125–146. [https://doi.org/10.1130/2005.2396\(09\)](https://doi.org/10.1130/2005.2396(09)).
- 893 Harris, A.J.L., Flynn, L.P., Matías, O., Rose, W.I., 2002. The thermal stealth flows of
894 Santiaguito dome, Guatemala: Implications for the cooling and emplacement of dacitic
895 block-lava flows. *Bull. Geol. Soc. Am.* 114, 533–546. [https://doi.org/10.1130/0016-7606\(2002\)114<0533:TTSFOS>2.0.CO;2](https://doi.org/10.1130/0016-7606(2002)114<0533:TTSFOS>2.0.CO;2)
- 897 Harris, A.J.L., Flynn, L.P., Matias, O., Rose, W.I., Cornejo, J., 2004. The evolution of an
898 active silicic lava flow field: an ETM + perspective 135, 147–168.
899 <https://doi.org/10.1016/j.jvolgeores.2003.12.011>
- 900 Harris, A.J.L., Rowland, S.K., 2009. Effusion Rate Controls on Lava Flow Length and the
901 Role of Heat Loss: A Review. *Leg. Georg. P.L. Walker, Spec. Publ. IAVCEI. Eds*
902 *Hoskuldsson A, Thordarson T, Larsen G, Self S, Rowl. S. Geol. Soc. London.* 2, 33–51.
- 903 Harris, A.J.L., Rowland, S.K., 2001. FLOWGO: a kinematic thermo-rheological model for
904 lava flowing in a channel. *Bull. Volcanol.* 63, 20–44.

- 905 <https://doi.org/10.1007/s004450000120>
- 906 Herault, A., Bilotta, G., Vicari, A., Rustico, E., Del Negro, C., 2011. Numerical simulation of
907 lava flow using a GPU SPH model. Del Negro, C. Gresta, S. Lava Flow Invasion Hazard
908 Map Mt. Etna Methods its Dyn. Updat. Ann. Geophys. 54.
- 909 Herault, A., Bilotta, G., Vicari, A., Rustico, E., Del Negro, C., 2009. Forecasting lava flow
910 hazards during the 2006 Etna eruption: Using the MAGFLOW cellular automata model.
911 J. Volcanol. Geotherm. Res. 112, 78–88. <https://doi.org/10.1016/j.cageo.2007.10.008>
- 912 Heslop, S.E., Wilson, L., Pinkerton, H., Head, J.W., 1989. Dynamics of a confined lava flow
913 on Kilauea Volcano, Hawaii. Bull. Volcanol. 51, 415–432.
- 914 Hess, K.-U., Dingwell, D.B., 1996. Viscosities of hydrous leucogranitic melts: {A non-
915 Arrhenian model}. Am. Mineral. 81, 1297–1300.
- 916 Hidaka, M., Goto, A., Umino, S., Fujita, E., 2005. VTFS project: development of the lava
917 flow simulation code LavaSIM with a model for three-dimensional convection,
918 spreading, and solidification. Geochemistry, Geophys. Geosystems 6, Q07008.
- 919 Hon, K., Gansecki, C., Kauahikaua, J., 2003. The transition from 'a'ā to pāhoehoe crust on
920 flows emplaced during the Pu'u Ō'ō-Kūpaianaha eruption. USGS Prof. Pap. 1676 89–
921 103. [https://doi.org/10.1016/0003-6870\(73\)90259-7](https://doi.org/10.1016/0003-6870(73)90259-7)
- 922 Hui, H., Zhang, Y., 2007. Toward a general viscosity equation for natural anhydrous and
923 hydrous silicate melts. Geochim. Cosmochim. Acta 71, 403–416.
- 924 Hulme, G., 1974. The Interpretation of Lava Flow Morphology. Geophys. J. R. Astron. Soc.
925 39, 361–383.
- 926 Ishibashi, H., Sato, H., 2007. Viscosity measurements of subliquidus magmas: Alkali olivine
927 basalt from the Higashi-Matsuura district, Southwest Japan. J. Volcanol. Geotherm. Res.
928 160, 223–238.
- 929 James, M.R., Pinkerton, H., Robson, S., 2007. Image-based measurement of flux variation in
930 distal regions of active lava flows. Geochemistry, Geophys. Geosystems 8.
931 <https://doi.org/10.1029/2006GC001448>
- 932 Jeffreys, H., 1925. The flow of water in an inclined channel of rectangular section. Philos.
933 Mag. serie 6, 4, 293,793-807.
- 934 Kelfoun, K., Vargas, S.V., 2016. VolcFlow capabilities and potential development for the
935 simulation of lava flows, in: Harris, A.J.L., De Groot, T., Garel, F., Carn, S.A. (Eds.),
936 Detecting, Modelling and Responding to Effusive Eruptions. Geological Society,
937 London, pp. 337–343. <https://doi.org/10.1144/SP426.8>

- 938 Kerr, R.C., Lyman, A.W., 2007. Importance of surface crust strength during the flow of the
939 1988-1990 andesite lava of Lonquimay Volcano, Chile. *J. Geophys. Res.* 112, B03209.
- 940 Keszthelyi, L., Self, S., 1998. Some physical requirements for the emplacement of long
941 basaltic lava flows. *J. Geophys. Res.* B11, 27,447-27,464.
- 942 Kilburn, C.R.J., Lopes, R.M.C., 1991. General patterns of flow field growth: 'A' and blocky
943 lavas. *J. Geophys. Res.* 96, 19721–19732. <https://doi.org/10.1029/91jb01924>
- 944 Klein, J., Mueller, S.P., Helo, C., Schweitzer, S., Gurioli, L., Castro, J.M., 2018. An expanded
945 model and application of the combined effect of crystal-size distribution and crystal
946 shape on the relative viscosity of magmas. *J. Volcanol. Geotherm. Res.* 357, 128–133.
947 <https://doi.org/10.1016/j.jvolgeores.2018.04.018>
- 948 Kolzenburg, S., Di Genova, D., Giordano, D., Hess, K.-U., Dingwell, D.B., 2018a. The effect
949 of oxygen fugacity on the rheological evolution of crystallizing basaltic melts. *Earth
950 Planet. Sci. Lett.* 487, 21–32. <https://doi.org/10.1016/j.epsl.2018.01.023>
- 951 Kolzenburg, S., Giordano, D., Cimarelli, S., Dingwell, D.B., 2016. In situ thermal
952 characterization of cooling/crystallizing lavas during rheology measurements and
953 implications for lava flow emplacement. *Geochim. Cosmochim. Acta* 195, 244–258.
- 954 Kolzenburg, S., Giordano, D., Hess, K.-U., Dingwell, D.B., 2018b. Shear-rate Dependent
955 Disequilibrium Rheology and Dynamics of Basalt Solidification. *Geophys. Res. Lett.*
956 <https://doi.org/doi.org/10.1029/2018GL077799>
- 957 Kolzenburg, S., Giordano, D., Thordarson, T., Hoskuldsson, A., Dingwell, D.B., 2017. The
958 rheological evolution of the 2014/2015 eruption at Holuhraun, central Iceland. *Bull.
959 Volcanol.* 79.
- 960 Kolzenburg, S., Jaenicke, J., Münzer, U., Dingwell, D.B., 2018c. The effect of inflation on
961 the morphology-derived rheological parameters of lava flows and its implications for
962 interpreting remote sensing data - A case study on the 2014/2015 eruption at Holuhraun,
963 Iceland. *J. Volcanol. Geotherm. Res.* 357, 200–212.
964 <https://doi.org/10.1016/j.jvolgeores.2018.04.024>
- 965 Kono, Y., 2018. Viscosity Measurement, in: *Magmas Under Pressure*. Elsevier, pp. 261–280.
966 <https://doi.org/10.1016/B978-0-12-811301-1.00010-1>
- 967 Krauskopf, K.B., 1948. Lava Mouvement at Paricutin Volcano, Mexico. *Geol. Soc. Am.
968 Bull.* 12, 1267–1284.
- 969 Krieger, I.M., Dougherty, T.J., 1959. A Mechanism for Non-Newtonian Flow in Suspensions
970 of Rigid Spheres. *J. Rheol. (N. Y. N. Y.)* 3, 137.

- 971 Larson, R.G., 1999. The structure and rheology of complex fluids. Oxford University Press,
972 New York.
- 973 Lavallée, Y., Hess, K.-U., Cordonnier, B., Dingwell, D.B., 2007. Non-Newtonian rheological
974 law for highly crystalline dome lavas. *Geology* 35, 843–846.
- 975 Lavallée, Y., Varley, N.R., Alatorre-Ibargüengoitia, M.A., Hess, K.-U., Kueppers, U.,
976 Mueller, S., Richard, D., Scheu, B., Spieler, O., Dingwell, D.B., 2012. Magmatic
977 architecture of dome-building eruptions at Volcán de Colima, Mexico. *Bull. Volcanol.*
978 74, 249–260.
- 979 Le Losq, C., Neuville, D.R., Moretti, R., Kyle, P.R., Oppenheimer, C., 2015. Rheology of
980 phonolitic magmas - the case of the Erebus lava lake. *Earth Planet. Sci. Lett.* 411, 53–61.
981 <https://doi.org/10.1016/j.epsl.2014.11.042>
- 982 Lefler, E., 2011. Genauigkeitsbetrachtung bei der Ermittlung rheologischer Parameter von
983 Lavaströmen aus Fernerkundungsdaten. Berlin, Freie Universität.
- 984 Lejeune, A.M., Bottinga, Y., Trull, T.W., P., R., 1999. Rheology of bubble-bearing magmas.
985 *Earth Planet. Sci. Lett.* 166, 71–84.
- 986 Lenk, R.S., 1967. A Generalized Flow Theory. *J. Appl. Polym. Sci.* 11, 1033–1042.
- 987 Lev, E., James, M.R., 2014. The influence of cross-sectional channel geometry on rheology
988 and flux estimates for active lava flows. <https://doi.org/10.1007/s00445-014-0829-3>
- 989 Lipman, P.W., Banks, N.G., 1987. Aa flow dynamics, Mauna Loa 1984. *U.S. Geol. Surv.*
990 Prof. Pap 1350 1527–1567.
- 991 Lipman, P.W., Banks, N.G., Rhodes, J.M., 1985. Degassing-induced crystallization of
992 basaltic magma and effects on lava rheology. *Nature* 317, 604–607.
- 993 Llewellyn, E.W., Manga, M., 2005. Bubble suspension rheology and implications for conduit
994 flow. *J. Volcanol. Geotherm. Res.* 143, 205–217.
- 995 Lunne, T., Robertson P.K., Powell, J.J.M., 1997. Cone Penetration Testing in Geotechnical
996 Practice. Blackie Academic/Chapman-Hall, U.K.
- 997 Mader, H.M., Llewellyn, E.W., Mueller, S.P., 2013. The rheology of two-phase magmas: A
998 review and analysis. *Bull. Volcanol.* 257, 135–158.
- 999 Manga, M., Castro, J., Cashman, K. V, M., L., 1998. Rheology of bubble-bearing magmas. *J.*
1000 *Volcanol. Geotherm. Res.* 87, 15–28.
- 1001 Maron, S.H., Pierce, P.E., 1956. Application of Ree-Eyring generalized flow theory to
1002 suspensions of spherical particles. *J. Colloid Sci.* 11, 80–95.
- 1003 Moitra, P., Gonnermann, H.M., 2015. Effects of crystal shape- and size-modality on magma

- 1004 rheology. *Geochemistry, Geophys. Geosystems* 16, 1–26.
- 1005 Moore, H.J., 1987. Preliminary estimates of the rheological properties of 1984 Mauna Loa
1006 Lava. *U.S. Geol. Surv. Prof. Pap.* 1350 99, 1569–1588.
- 1007 Moore, H.J., Schaber, G.G., 1975. An estimate of the yield strength of the Imbrium flows.
1008 *Proceeding Lunar Sci. Conf.* 6th, 101–118.
- 1009 Mossoux, S., Saey, M., Bartolini, S., S., P., Canters, F., Kervyn, M., 2016. Q-LAVHA: A
1010 flexible GIS plugin to simulate lava flows. *Comput. Geosci.* 97, 98–109.
- 1011 Mueller, S., Llewellyn, E.W., Mader, H.M., 2010. The rheology of suspensions of solid
1012 particles. *Philos. Trans. R. Soc. Lond. A* 466, 1201–1228.
- 1013 Nichols, R.L., 1939. Viscosity of Lava. *J. Geol.* 47, 290–302.
- 1014 Norton, G., Pinkerton, H., 1997. Rheological properties of natrocarbonatite lavas from
1015 Oldoinyo Lengai, Tanzania. *Eur. J. Mineral.* 9, 351–364.
- 1016 Panov, V.K., Slezin, Y.B., Storcheus, A. V, 1988. Mechanical properties of lavas extruded in
1017 the 1983 Predskazannyi eruption (Klyuchevskoy volcano). *Volcanol. Seismol.* 7, 25–37.
- 1018 Panov, V.K., Slezin, Y.B., Storcheus, A. V, 1985. Mechanical properties of lavas of flank
1019 eruption Predskazanny (Predicted), 1983, Klyuchevskoy volcano. *J. Volcanol. Seismol.*
1020 *Russ.* 1, 21–28.
- 1021 Phan-Thien, N., Pham, D.C., 1997. Differential multiphase models for polydispersed
1022 suspensions and particulate solids. *J. Nonnewton. Fluid Mech.* 72, 305–318.
- 1023 Pinkerton, H., 1994. Rheological and related properties of lavas, in: F. Dobran (Ed.), *Etna:
1024 Magma and Lava Flow Modeling and Volcanic System Definition Aimed at Hazard
1025 Assessment. Global Volcanic And Environmental System Simulation*, pp. 76–89.
- 1026 Pinkerton, H., 1978. *Methods of Measuring the Rheological Properties of Lava.* University of
1027 Lancaster.
- 1028 Pinkerton, H., Herd, R.A., Kent, R.M., Wilson, L., 1995b. Field measurements of the
1029 rheological properties of basaltic lavas. *Lunar Planet. Sci.* XXVI, 1127–1128.
- 1030 Pinkerton, H., Norton, G., 1995. Rheological properties of basaltic lavas at sub-liquidus
1031 temperatures: laboratory and field measurements on lavas from Mount Etna. *J. Volcanol.*
1032 *Geotherm. Res.* 68, 307–323.
- 1033 Pinkerton, H., Norton, G., 1983. A comparison of calculated and measured rheological
1034 properties of crystallizing lavas in the field and in the laboratory, in: *Lunar and Planetary
1035 Science XXIV*. pp. 1149–1150.
- 1036 Pinkerton, H., Norton, G.E., Dawson, J.B., Pyle, D.M., 1995a. Field observations and

- 1037 measurements of the physical properties of Oldoinyo Lengai alkali carbonatite lavas,
1038 November 1988, in: Bell, K., Keller, J. (Eds.), IAVCEI Proceedings in Volcanology 4.
1039 Carbonatite Volcanism of Oldoinyo Lengai - Petrogenesis of Natrocarbonatite. Springer-
1040 Verlag, Berlin, pp. 23–36.
- 1041 Pinkerton, H., Sparks, R.S.J., 1978. Field measurements of the rheology of lava. *Nature* 276,
1042 383–385.
- 1043 Pinkerton, H., Stevenson, R.J., 1992. Methods of determining the rheological properties of
1044 magmas at sub-liquidus temperatures. *J. Volcanol. Geotherm. Res.* 53, 47–66.
- 1045 Pinkerton, H., Wilson, L., 1994. Factor controlling the lengths of channel-fed lava flows.
1046 *Bull. Volcanol.* 6, 108–120.
- 1047 Pistone, M., Caricchi, L., Ulmer, P., Burlini, L., Ardia, P., Reusser, E., Marone, F., L., A.,
1048 2012. Deformation experiments of bubble- and crystal-bearing magmas: Rheological and
1049 microstructural analysis. *J. Geophys. Res.* 117, B05208.
- 1050 Pistone, M., Caricchi, L., Ulmer, P., Reusser, E., Ardia, P., 2013. Rheology of volatile-
1051 bearing crystal mushes: Mobilization vs. viscous death. *Chem. Geol.* 345, 16–39.
1052 <https://doi.org/10.1016/j.chemgeo.2013.02.007>
- 1053 Pistone, M., Cordonnier, B., Ulmer, P., Caricchi, L., 2016. Rheological flow laws for
1054 multiphase magmas: An empirical approach. *J. Volcanol. Geotherm. Res.* 321, 158–170.
1055 <https://doi.org/10.1016/j.jvolgeores.2016.04.029>
- 1056 Plechov, P., Blundy, J., Nekrylov, N., Melekhova, E., Shcherbakov, V., Tikhonova, M.S.,
1057 2015. Petrology and volatile content of magmas erupted from Tolbachik Volcano,
1058 Kamchatka, 2012-13. *J. Volcanol. Geotherm. Res.* 307, 182–199.
1059 <https://doi.org/10.1016/j.jvolgeores.2015.08.011>
- 1060 Ramsey, M., Chevrel, M.O., Coppola, D., Harris, A.J.L., 2019. The influence of emissivity
1061 on the thermo-rheologic al modeling of the channelized lava flows at Tolbachik volcano.
1062 *Ann. Geophys.* 61.
- 1063 Rhéty, M., Harris, A.J.L., Villeneuve, N., Gurioli, L., Médard, E., Chevrel, M.O., Bachèlery,
1064 P., 2017. A comparison of cooling-limited and volume-limited flow systems: Examples
1065 from channels in the Piton de la Fournaise April 2007 lava-flow field. *Geochemistry,*
1066 *Geophys. Geosystems* 18, 3270–3291. <https://doi.org/10.1002/2017GC006839>
- 1067 Riker, J.M., Cashman, K. V., Kauahikaua, J.P., Montierth, C.M., 2009. The length of
1068 channelised lava flows: insight from the 1859 eruption of Mauna Loa Volcano, Hawaii.
1069 *J. Volcanol. Geotherm. Res.* 183, 139–156.

- 1070 Robert, B., Harris, A., Gurioli, G., Medard, E., Sehlke, A., Whittington, A., 2014. Textural
1071 and rheological evolution of basalt flowing down a lava channel. *Bull. Volcanol.* 76,
1072 824.
- 1073 Rose, W.I., 1973. Pattern and mechanism of volcanic activity at the Santiaguito Volcanic
1074 Dome, Guatemala. *Bull. Volcanol.* 37, 73–94. <https://doi.org/10.1007/BF02596881>
- 1075 Rust, A.C., Manga, M., 2002. Bubble shapes and orientations in low Re simple shear flow.,
1076 *Journal Colloid Interface Sci.* 249, 476–480.
- 1077 Ryerson, F.J., Weed, H.C., Piwinski, A.J., 1988. Rheology of subliquidus magmas: Picritic
1078 compositions. *J. Geophys. Res.* 93, 3421–3436.
- 1079 Saar, M.O., Manga, M., 1999. Permeability-porosity relationship in vesicular basalts.
1080 *Geophys. Res. Lett.* 26, 111–114.
- 1081 Sato, H., 2005. Viscosity measurement of subliquidus magmas: 1707 basalt of {F}uji
1082 volcano. *J. Mineral. Petrol. Sci.* 100, 133–142.
- 1083 Sehlke, A., Whittington, A., Robert, B., Harris, A.J.L., Gurioli, L., Médard, E., 2014.
1084 Pahoehoe to `a`a transition of Hawaiian lavas: an experimental study. *Bull. Volcanol.* 76,
1085 876.
- 1086 Sehlke, A., Whittington, A.G., 2016. The viscosity of planetary tholeiitic melts: A
1087 configurational entropy model. *Geochim. Cosmochim. Acta* 191, 277–299.
- 1088 Shaw, H.R., 1972. Viscosities of magmatic silicate liquids: An empirical method of
1089 prediction. *Am. J. Sci.* 272, 870–893.
- 1090 Shaw, H.R., Wright, T.L., Peck, D.L., Okamura, R., 1968. The Viscosity of Basaltic Magma:
1091 An analysis of Field Measurements in Makaopuhi Lava Lake, Hawaii. *Am. J. Sci.* 266,
1092 225–264.
- 1093 Smith, J. V, 2000. Textural evidence for dilatant (shear thickening) rheology of magma at
1094 high crystal concentrations. *J. Volcanol. Geotherm. Res.* 99, 1–7.
- 1095 Smith, J. V, 1997. Shear thickening dilatancy in crystal-rich flows. *J. Volcanol. Geotherm.*
1096 *Res.* 79, 1–8.
- 1097 Soldati, A., Sehlke, A., Chigna, G., Whittington, A., 2014. Field and experimental constraints
1098 on the rheology of arc basaltic lavas: the January 2014 Eruption of Pacaya (Guatemala).
1099 *Bull. Volcanol.* 78.
- 1100 Sólnes J, Á. Ásgeirsson, B. Bessason, and F. Sigmundsson. Náttúruvá Á Íslandi, Eldgos og
1101 Jarðskjálftar. Reykjavík: Viðlagatrygging/ Háskólaútgáfan, 2013
- 1102 Soule, S.A., Cashman, K.V., Kauahikaua, J.P., 2004. Examining flow emplacement through

- 1103 the surface morphology of three rapidly emplaced, solidified lava flows, Kīlauea
1104 Volcano, Hawai'i. *Bull. Volcanol.* 66, 1–14. <https://doi.org/10.1007/s00445-003-0291-0>
- 1105 Spera, F.J., Borgia, A., Strimple, J., Feigenson, M., 1988. Rheology of melts and magmatic
1106 suspensions I. Design and calibration of a concentric cylinder viscometer with
1107 application to rhyolitic magma. *J. Geophys. Res.* 93, 10273–10294.
- 1108 Stein, D.J., Spera, F.J., 1998. New high-temperature rotational rheometer for silicate melts,
1109 magmatic suspensions, and emulsions. *Rev. Sci. Instrum.* 69, 3398–3402.
1110 <https://doi.org/doi:10.1063/1.1149106>
- 1111 Stein, D.J., Spera, F.J., 1992. Rheology and microstructure of magmatic emulsions: Theory
1112 and experiments. *J. Volcanol. Geotherm. Res.* 49, 157–174.
- 1113 Vetere, F., Iezzi, G., Behrens, H., Holtz, F., Ventura, G., Misiti, V., Cavallo, A., Mollo, S.,
1114 Dietrich, M., 2015. Glass forming ability and crystallisation behaviour of sub-alkaline
1115 silicate melts. *Earth-Science Rev.* 150, 25–44.
1116 <https://doi.org/10.1016/j.earscirev.2015.07.001>
- 1117 Vetere, F., Sato, H., Ishibashi, H., De Rosa, R., Donato, P., Ishebashi, H., De Rosa, R.,
1118 Donato, P., 2013. Viscosity changes during crystallization of a shoshonitic magma: new
1119 insights on lava flow emplacement. *J. Mineral. Petrol. Sci.* 108, 144–160.
1120 <https://doi.org/10.2465/jmps.120724>
- 1121 Vicari, A., Bilotta, G., Bonfiglio, S., Cappello, A., Ganci, G., Herault, A., Rustico, E., Gallo,
1122 G., Del Negro, C., 2011. Lav@hazard: A web-gis interface for volcanic hazard
1123 assessment. *Ann. Geophys.* 54, 662–670. <https://doi.org/10.4401/ag-5347>
- 1124 Vicari, A., Herault, A., Del Negro, C., Coltelli, M., Marsella, M., Proietti, C., 2007. Modeling
1125 of the 2001 lava flow at Etna volcano by a Cellular Automata approach. *Environ. Model.*
1126 *Softw.* 22, 1465–1471.
- 1127 Vona, A., Di Piazza, A., Nicotra, E., Romano, C., Viccaro, M., Giordano, G., 2017. The
1128 complex rheology of megacryst-rich magmas: The case of the mugearitic “cicirara” lavas
1129 of Mt. Etna volcano. *Chem. Geol.* 458, 48–67.
1130 <https://doi.org/10.1016/j.chemgeo.2017.03.029>
- 1131 Vona, A., Romano, C., 2013. The effects of undercooling and deformation rates on the
1132 crystallization kinetics of Stromboli and Etna basalts. *Contrib. to Mineral. Petrol.* 166,
1133 491–509. <https://doi.org/10.1007/s00410-013-0887-0>
- 1134 Vona, A., Romano, C., Dingwell, D.B., Giordano, D., 2011. The rheology of crystal-bearing
1135 basaltic magmas from Stromboli and Etna. *Geochim. Cosmochim. Acta* 3214–3236.

- 1136 Vona, A., Romano, C., Giordano, D., Russell, J.K., 2013. The multiphase rheology of
1137 magmas from Monte Nuovo (Campi Flegrei, Italy). *Chem. Geol.* 346, 213–227.
1138 <https://doi.org/10.1016/j.chemgeo.2012.10.005>
- 1139 Vona, A., Ryan, A.G., Russell, J.K., Romano, C., 2016. Models for viscosity and shear
1140 localization in bubble-rich magmas. *Earth Planet. Sci. Lett.* 449, 26–38.
1141 <https://doi.org/10.1016/j.epsl.2016.05.029>
- 1142 Wadge, G., Lopes, R.M.C., 1991. The lobes of lava flows on Earth and Olympus Mons, Mars.
1143 *Bull. Volcanol.* 6, 10–24.
- 1144 Walker, G.P.L., 1973. Lengths of lava flows. *Philos. Trans. R. Soc. London* 274, 107–118.
- 1145 Woodcock, D., Harris, A., 2006. The dynamics of a channel-fed lava flow on Pico Partido
1146 volcano, Lanzarote. *Bull. Volcanol.* 69, 207–215. [https://doi.org/10.1007/s00445-006-](https://doi.org/10.1007/s00445-006-0068-3)
1147 [0068-3](https://doi.org/10.1007/s00445-006-0068-3)
- 1148